EUROPEAN ORGANIZATION FOR NUCLEAR RESEARCH

CERN - LABORATORY II

CERN LAB II/BT/74-1

EXTERNAL TARGETS AT THE SPS

W. Kalbreier, W.C. Middelkoop, P. Sievers

Abstract:

A study is made of the thermal effects which occur in external targets when irradiated by fast and slow extracted SPS beams of 400 GeV/c, 10^{13} protons per pulse and a beam diameter of 2 mm. The temperature and the thermal stress distributions are derived from the longitudinal and radial distributions of the energy deposition density in the materials Be, BeO, B_4C, C, SiC, Al, Al_2O_3, Ti, Cu, Mo and W. For several of these materials the maximum temperature during the burst and the steady-state temperatures are calculated for targets cooled by either radiation, forced gas convection or conduction.

The dynamic thermal stress created in a target due to its rapid heating in fast extracted beams can be reduced to values sufficiently below the yield strength of the materials by a subdivision of the total target length into several parts. In fast extracted beams the quasi-static thermal stress which is produced in a target due to the radial temperature gradient will exceed the elastic limit for all considered materials. For burst durations longer than about 50 ms the quasi-static thermal stress will become negligible.

Geneva - February, 1974

CONTENTS

1. Introduction

High-energy protons incident on a target generate hadronic and electromagnetic cascades which deposit part of the kinetic energy of the incoming proton beam in the target material. This energy deposition causes heating of the target. The main problem for external targets used in slow and fast extracted proton beams is therefore the cooling of the target. In addition, for fast extraction, the rapid temperature rise of the target causes thermal shock [1,2] and the non-uniform heating over its cross-section gives rise to quasi-static thermal stress [3].

In this report, calculations of the temperature and stress distributions produced in external targets are made for a proton beam of 400 GeV/c with an intensity of 10^{13} ppp, a cycle time of 4.77 s and a burst length of 23 μs for fast and of 700 ms for slow extraction[4]. A Gaussian beam profile has been assumed for the proton density distribution. The beam size is chosen in a way that 92% of the protons are contained in an area with a diameter of 2 mm (Appendix I). These rather extreme conditions will cause the highest target temperatures and stresses which could occur at the SPS.

2. Calculation of the energy deposition density

The local energy deposition density in the target has been calculated with a Monte Carlo programme in which the development of nucleon-meson cascades is simulated [5]. The computed energy deposition density E is given in GeV cm^{-3} per incoming proton of 400 GeV/c for the beam size defined above *).

The Monte Carlo programme gives the distribution of the energy deposition density and therefore also the temperature distribution at the time when the nucleon-meson cascade has deposited its energy in the

---

*) 1 GeV = $1.60 \cdot 10^{-3}$ erg = $3.82 \cdot 10^{-11}$ cal.

target. It does not include the time-dependent variation of the temperature distribution inside the target due to thermal diffusion.

The Monte-Carlo calculations are made for thin cylindrical targets with a length of one interaction mean-free path [6]. Values of this latter parameter are given in Table I for several target materials. To optimize the target efficiency, i.e. the number of secondaries per interacting proton, materials of low atomic weight must be selected.

Target material		Interaction length	
		g cm^{-2}	cm
beryllium	Be	66	36
beryllia	BeO	74	26
boron carbide	B_4C	73	29
graphite	C	79	46
silicon carbide	SiC	87	28
aluminium	Al	95	35
alumina	Al_2O_3	87	22
titanium	Ti	115	26
copper	Cu	124	14
molybdenum	Mo	144	14
tungsten	W	191	10

TABLE I

Interaction lengths for several target materials

Figure 1 shows the radial and longitudinal distribution of the energy deposition density in a beryllium target. For beryllium and also for other target materials of low mass density, the energy deposition density

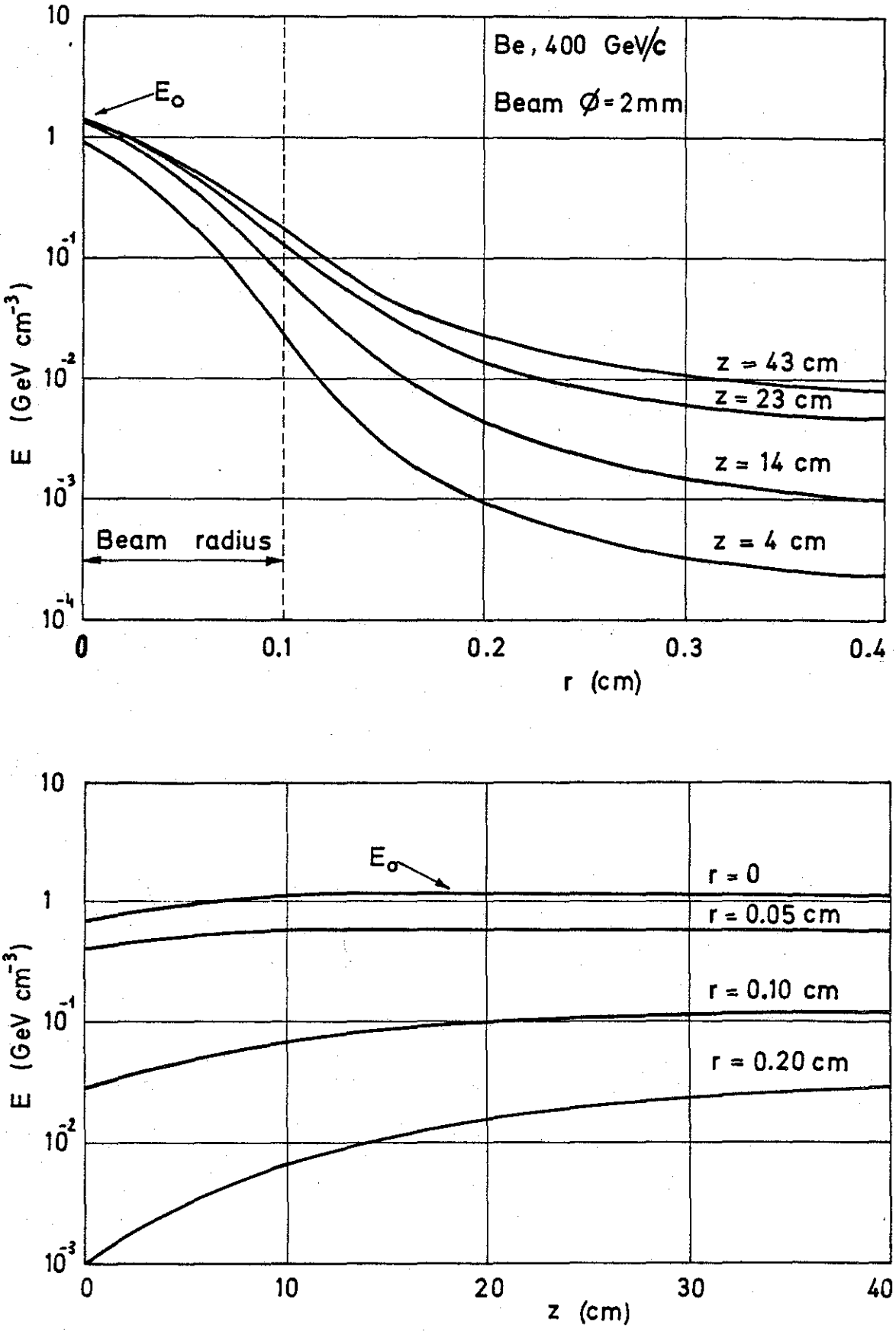

Fig. 1 For a Gaussian distribution of the proton intensity the energy deposition density E per incoming proton is shown for a Be-target as a function of

i) the radial distance r at different depths z
ii) the longitudinal co-ordinate z at different values of r.

The maximum energy deposition density E_o obtained at the target axis is also indicated.

remains about constant along the target axis, whereas for materials of a high mass density a maximum is reached at a certain depth within the target length.

The evaluation of the target temperatures in this report is always made under the assumption that the longitudinal distribution of the energy deposition density calculated with the Monte Carlo programme is represented by a constant value corresponding to the maximum value obtained. Similarly, that radial distribution of the energy deposition density is taken which after integration over the target radius gives the maximum deposited heat.

The maximum of the longitudinal distribution of the energy deposition density obtained along the target axis is called E_o. For a given target material the value of E_o depends strongly on the proton density distribution of the incident beam [7].

The uncertainty of the calculated distribution of the energy deposition produced by high-energy protons in external targets results mainly from two sources. Firstly, it cannot be excluded that the assumed gaussian distribution of the proton intensity which enters the Monte Carlo simulation programme differs substantially from the true beam profile. Secondly, the uncertainty in the parameters governing the cascade calculations of the Monte Carlo programme is estimated to be 50% or less [8].

3. One beam pulse incident on an external target

3.1 The target temperature due to heating and thermal diffusion

3.1.1 The characteristic thermal diffusion time

The local temperature rise per incoming proton which occurs adiabatically in the target can be evaluated from the local energy deposition density with the following formula

$$T(r) = 3.82 \cdot 10^{-11} \frac{E(r)}{\rho \, c_p} \qquad (1)$$

where

r : radial co-ordinate (cm)
T(r) : local temperature rise per incoming proton (°C)
E(r) : local energy deposition density per incoming proton (GeV cm^{-3})
c_p : specific heat (cal g^{-1} $°C^{-1}$)
ρ : mass density (g cm^{-3})

For the evaluation of the adiabatic temperature rise with Eq. (1) the specific heat is always taken at 25°C. The increase of c_p with temperature is neglected which gives pessimistic values for the calculated temperatures.

For a beam pulse of infinitesimal duration incident on a target, the heating proceeds adiabatically since the thermal diffusion can be neglected. Thus, the distribution of the temperature rise has the same shape as the energy deposition density calculated by the Monte-Carlo programme.

For a finite duration τ of the beam pulse these distributions are spread out by thermal diffusion already during the burst. The time in which the heat is about uniformly distributed over the zone initially heated by the beam can be estimated from a special case where a line source deposits heat instantaneously in an infinite body. Then the radial evolution of the temperature due to thermal diffusion is given by the following formula

$$T(r,t) = \frac{Q_\ell}{4\pi\lambda t} \exp\left(-\frac{r^2}{4at}\right) \qquad (2)$$

where

t : time (s)
a : thermal diffusivity ($= \frac{\lambda}{c_p \cdot \rho}$)
λ : thermal conductivity (cal $cm^{-1} s^{-1} °C^{-1}$)
Q_ℓ : heat produced instantaneously per cm by a proton beam at t = 0 (cal/cm).

The zone around the target axis which is heated considerably by the beam is limited approximately by the beam radius R_b as shown further below in Fig. 2.

Therefore, the characteristic thermal diffusion time t_{diff} is defined here as the time necessary for the r.m.s. value σ of Eq. (2) to become equal to the beam radius of R_b = 1 mm.

$$\sigma = \sqrt{2at_{diff}} \approx R_b \ .$$

In Table II the characteristic thermal diffusion time is given for several target materials and a beam radius of 1 mm.

Target Material	Thermal conductivity ++) (cal cm^{-1} s^{-1} $°C^{-1}$)	t_{diff} (ms)
Be	0.36	11
BeO	0.57	6
B_4C	0.074	32
C +)	0.11	13
SiC	0.21	25
Al	0.55	5
Al_2O_3	0.08	45
Ti	0.047	60
Cu	0.95	4
Mo	0.33	9
W	0.43	7

+) graphite ++) at 25 °C

TABLE II

The characteristic thermal diffusion time t_{diff} is given for several target materials and a beam radius of 1 mm.

3.1.2 The temperature rise due to one slow extracted pulse

Table II shows for slow extraction, when thin targets of a diameter comparable with the beam diameter will be used, that the characteristic thermal diffusion time is short compared with an assumed burst duration of 700 ms. Thus, although the heat is non-uniformly deposited in the radial direction of the target, no significant radial temperature gradient is created during the burst. Moreover, the heating is no longer adiabatic and the temperature increase reached at the end of a burst will already be reduced by the cooling during the burst as will be discussed in section 5.2.1.

In the absence of cooling, the average temperature $\overline{T}$, reached in the target at the end of a slow extracted pulse, can be calculated from the energy deposition density averaged over the target cross-section. The values of $\overline{T}$ are given in Table III for targets of 2 mm and 4 mm diameter irradiated by a proton pulse of 400 GeV/c, 10^{13} ppp and a beam diameter of 2 mm. They will be used later for the calculation of the target temperatures obtained with cooling. For comparison also the melting points T_{melt} are given for the listed target materials.

Table III shows that for the target materials Cu, Mo and W which are initially kept e.g. at room temperature even the average temperature rise $\overline{T}$ reached at the end of one slow extracted pulse in the absence of cooling exceeds the melting point except for the Mo-target of 4 mm diameter. Therefore, these and also other materials of high atomic weight will not be further considered in this report.

3.1.3 The temperature rise due to one fast extracted pulse

For a fast extracted pulse Table II shows that the thermal diffusion velocity is far too low to distribute the deposited heat uniformly over the heated zone of the target during a burst duration of $\tau \leq 23$ μs. Therefore, the target heating proceeds adiabatically and the temperature distribution is obtained directly from the distribution of the heat when deposited by the beam. Furthermore, a quasi-static temperature gradient is created in the radial direction of the target which due to thermal diffusion decreases for $t > \tau$ and vanishes for $t \approx t_{diff}$.

Target material	density ($g\ cm^{-3}$)	Specific heat ++) ($cal\ g^{-1}\ °C^{-1}$)	E_o ($GeV\ cm^{-3}$)	$\overline{T}$ (°C)		T_o (°C)	T_{melt} (°C)
				d = 2mm	d = 4 mm		
Be	1.85	0.436	1.06	190	60	490	1280
BeO	2.85	0.24	1.71	420	140	950	2570
B_4C	2.52	0.19	1.5	550	170	1190	2430
C +)	1.70	0.17	0.95	510	160	1250	3320*)
SiC	3.10	0.34	2.34	310	100	840	2700
Al	2.70	0.215	1.70	400	130	670	660
Al_2O_3	3.9	0.185	2.0	450	180	1060	2040
Ti	4.51	0.125	2.6	1070	450	1670	1670
Cu	8.96	0.092	7.5	1910	1080	2900	1080
Mo	10.24	0.06	16.7	4000	2500	9300	2610
W	19.3	0.032	65.6	20 000	8 800	39 000	3380

+) graphite ++) at 25°C *) sublimation point

TABLE III

For one beam pulse of 400 GeV/c, 10^{13} ppp, and a beam diameter of 2 mm, incident on different target materials, the maximum energy deposition density E_o is given. T_o is the maximum temperature rise in the centre of the target for the case of a fast extracted beam. The average temperature rise $\overline{T}$ reached in the target at the end of a slow extracted pulse in the absence of cooling, is calculated from the energy deposition density averaged over the target cross-section. The values of $\overline{T}$ are given for targets of 2 mm and 4 mm diameter. In order to compare the temperature of the target with the melting point T_{melt} its initial temperature must still be added to the given temperature rise.

For a fast extracted pulse of 400 GeV/c, 10^{13} ppp, and a beam diameter of 2 mm the maximum temperature rise T_o which occurs adiabatically along the target axis is computed from the maximum energy deposition density E_o. For several target materials values of T_o are given in Table III. If a target at room temperature is heated by one fast extracted pulse then for the materials Al and Ti and especially for those of a high atomic number like Cu, Mo and W the maximum target temperature T_o obtained along the target axis at the end of the burst reaches or even exceeds the melting point. Therefore, these materials cannot be used for external targets at the SPS if fast extracted beams with an intensity of 10^{13} ppp and a narrow waist must be focussed onto the target.

3.2 Thermal stress in external targets

3.2.1 Quasi-static and dynamic thermal stresses

In a freely suspended target which is slowly and uniformly heated, no thermal stress will occur. A non-uniform heating of the elastic target material gives rise to thermal stress, which will be called here quasi-static stress as the temperature distribution changes with time due to thermal diffusion. In a target heated by a proton burst the maximum of the quasi-static stress is reached at the end of the pulse. Its magnitude depends on the distribution of the heat when deposited by the beam and the duration of the heating period given by the burst length.

In slow extraction with pulses longer than about 50 ms the quasi-static thermal stress becomes negligible, since the characteristic thermal diffusion time given in Table II is of the order of 10 ms to 60 ms for the considered target materials. Recent calculations [9] have shown that extracted pulses of a few ms duration may be feasible. For burst lengths below about 50 ms the quasi-static thermal stress will become more important with decreasing burst duration.

In fast extraction with a pulse duration of 23 μs or shorter, the heating time is short compared with the characteristic thermal diffusion time and therefore the maximum values of the quasi-static stress are

reached, which are possible for a given beam profile and intensity.

In fast extraction the heating time is of the same order of magnitude as the propagation time of sound to traverse the target longitudinally, if its length is about one interaction mean-free path. Therefore, in addition to the quasi-static stress, dynamic stresses [1,2] are generated as a result of the fact that the target material cannot expand as rapidly as it is heated, due to its inertia. This latter phenomenon is commonly referred to as thermal shock. Longitudinal stress waves are created at both end-faces which propagate into the target with the velocity of sound. The maximum compressive and tensile stresses may easily lead to a destruction of the target as shown later in this report.

Since the target diameters are of the order of a few millimetres up to a maximum of about 1 cm, the heating time τ is long compared with the propagation time of sound to traverse the target in transverse direction. Therefore, radially the dynamic stress can be neglected [2].

In this report, in general, a spill time of about 700 ms is assumed for slow extraction for the sake of simplicity. This permits to distinguish between target operation for slow and fast extraction in a way that both the dynamic and the quasi-static thermal stress can be neglected for slow extraction. However, for the "fast slow extraction" with burst lengths between a few ms and about 50 ms, the provisions described in section 5.3 to overcome the quasi-static thermal stress produced in fast extraction must be applied.

3.2.2 Reduction of the dynamic thermal stress

The radial distribution of the temperature rise in external targets obtained from the Monte Carlo programme, and shown for beryllium in Fig.2, can be approximated by a linear function which decreases from the maximum temperature rise T_o at the target centre to zero at the radial distance R' and is then constant up to the target surface :

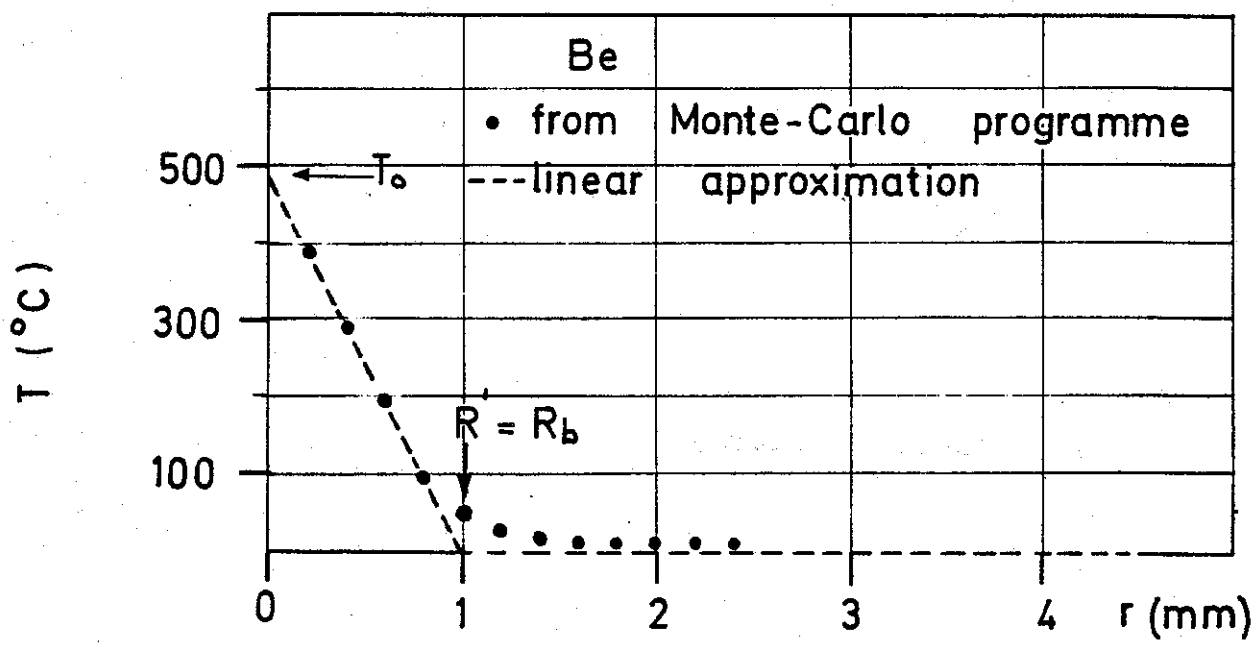

Fig. 2 The radial distribution of the temperature rise due to one fast extracted pulse of 400 GeV/c, 10^{13} ppp, and a beam radius of R_b = 1 mm is shown in Be-target. The maximum temperature rise T_o is obtained at the target axis.

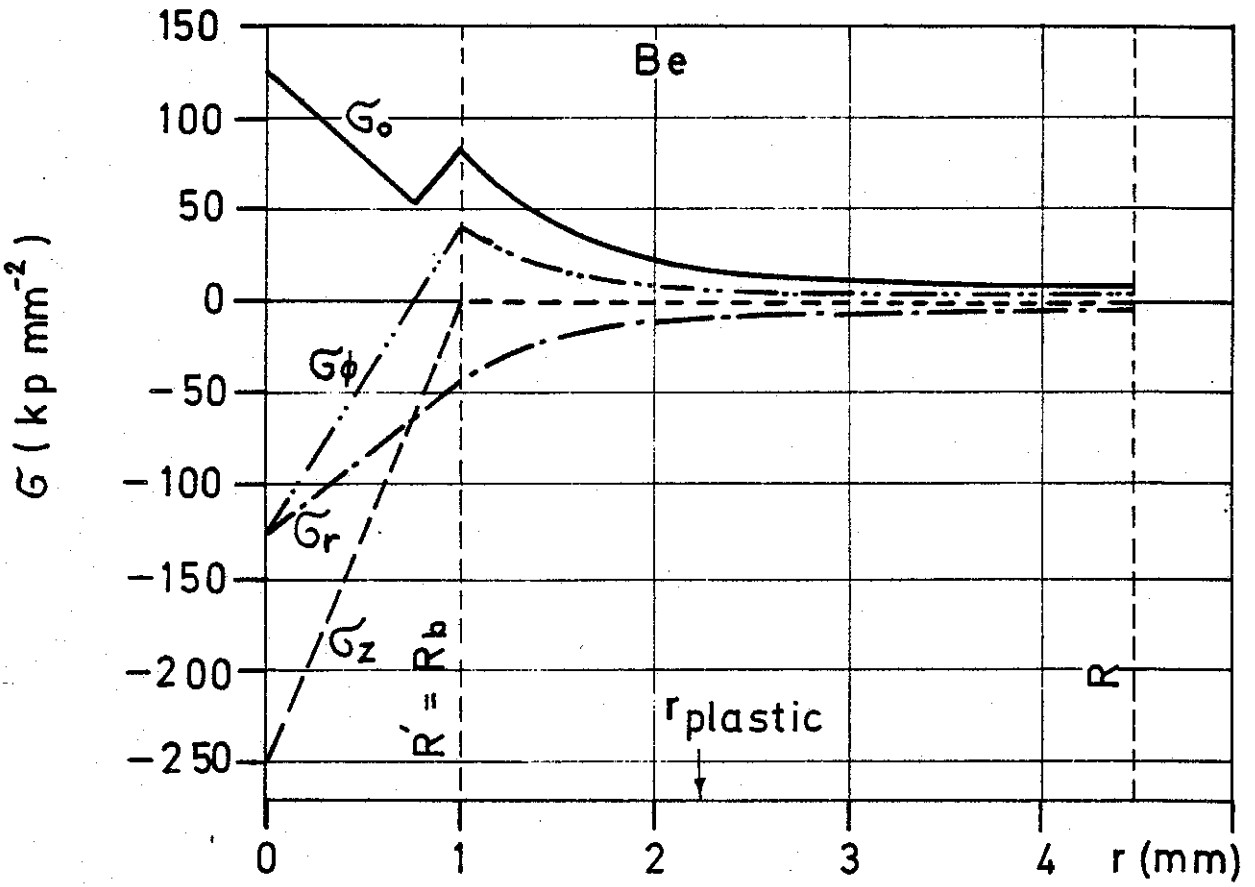

Fig. 3 The radial dependence of the stresses σ_ϕ, σ_r, σ_z and σ_o is shown for a Be-target of 9 mm diameter. For the stress calculation the linear approximation of the radial temperature distribution (dashed line in Fig. 2) has been applied. The radius of the plastic core around the target axis $r_{plastic}$ is also indicated for a yield strength of $\sigma_{0.2}$ = 14 kp mm^{-2}.

$$T(r) = \begin{cases} T_o\left(1 - \frac{r}{R'}\right) & 0 \leq r \leq R' \\ 0 & R' \leq r \leq R \end{cases}$$

In the case of a Gaussian distribution of the proton intensity characterized by a beam radius of 1 mm (see Appendix I), the range R' of the linear decreasing temperature coincides approximately with this value. With this approximation of the radial temperature distribution, the maxima of the dynamic (σ_z^{dyn}) and the quasi-static stress (σ_z^{stat}) in slender targets, as obtained for R ≈ R' in Appendix II, are given by

$$\sigma_z^{dyn} \approx \pm 1/3 \; E \; \alpha \; T_o$$

and

$$\sigma_z^{stat} \approx - E \; \alpha \; T_o$$

where α denotes the linear coefficient of thermal expansion and E is Young's modulus, when used in formulae for the thermal stress. (The symbol E should, of course, not be confused with the symbol E for the energy deposition density in the preceding part of this report). The ratio of the dynamic to the quasi-static stress is then :

$$\frac{\sigma_z^{dyn}}{\sigma_z^{stat}} \approx \pm \frac{1}{3}$$

The magnitude of the maximum dynamic stress depends on the target length ℓ in the following way [1,2]:

$$\sigma_z^{dyn} \cong \begin{cases} \pm 1/3 \; E \; \alpha \; T_o & \text{for } \ell \geq \tau \, v_{sound} \\ \pm 1/3 \; E \; \alpha \; T_o \; \frac{\ell}{v_{sound} \, \tau} & \text{for } \ell \leq \tau \, v_{sound} \end{cases}$$

where $v_{sound} = \sqrt{E/\rho}$ is the velocity of sound in a given target material, and τ is the heating time defined by the burst length. The target length ℓ will be typically one interaction length (see Table I).

Thus, by cutting the target longitudinally into several parts, the axial dynamic stress can be reduced accordingly, whereas, of course, the quasi-static stress is not changed. Table IV gives the target length ℓ_{10} for various materials for which the dynamic stress σ_z^{dyn} is decreased to 10% of the maximum quasi-static stress σ_z^{stat} .

target material	Be	BeO	B_4C	C	SiC	Al	Al_2O_3	Ti
ℓ_{10} (cm)	9.8	7.9	8.3	2.0	7.5	3.2	5.6	3.4
ℓ_{total} (cm)	36	26	29	46	28	35	22	26

TABLE IV : The length of the target segments ℓ_{10} for which the dynamic stress σ_z^{dyn} is reduced to 10% of the quasi-static stress σ_z^{stat} is given for several target materials. For comparison, also the interaction lengths are listed as typical lengths ℓ_{total} of the whole target.

3.2.3 Quasi-static thermal stress and the radius of the plastic core

Also for the calculation of the quasi-static thermal stress (see Appendix II) the linear approximation of the radial temperature distribution of the previous section has been applied.

Let σ_ϕ, σ_r, and σ_z denote the circumferential, radial, and longitudinal stress components, respectively, then the following relation holds :

$$0 \leq r \lesssim 3/4\ R' \qquad \sigma_\phi \geq \sigma_r \geq \sigma_z$$

$$3/4\ R' \lesssim r \leq R \qquad \sigma_\phi \geq \sigma_z \geq \sigma_r$$

Figure 3 shows the radial dependence of the stress components σ_ϕ, σ_r, and σ_z for the case of a beryllium target with $T_o = 490°C$, $R' = 1.0$ mm, and $R = 4.5$ mm.

According to the maximum shear theory [3], a material becomes plastic if the maximum difference σ_o between any two of the three stress components reaches the yield strength $\sigma_{0.2}$. For the linear approximation of the radial temperature distribution considered in this section σ_o is given by :

$$\sigma_o = \begin{cases} | \sigma_\phi - \sigma_z | & \text{for} \quad 0 \leq r \lesssim 3/4\ R' \\ | \sigma_\phi - \sigma_r | & \text{for} \quad 3/4\ R' \lesssim r \leq R \end{cases}$$

The radial distance for which σ_o becomes equal to the yield strength $\sigma_{0.2}$ is defined as the radius of the plastic core $r_{plastic}$. Then, for $r > r_{plastic}$ Hooke's law is still valid, whereas for $r < r_{plastic}$ the material is overstressed. The radial distribution of the stress σ_o is also shown in Fig. 3.

Table V gives the values of the plastic radii for several target materials which are evaluated from the following formula derived in Appendix II with the linear approximation of the radially decreasing temperature distribution

$$r_{plastic} = R' \sqrt{1/3 \frac{E\ \alpha\ T_o}{(1 - \nu)\sigma_{0.2}}}\ , \qquad (3)$$

where ν is Poisson's ratio.

target material	Be	BeO	B_4C	C	SiC	Al	Ti
$r_{plastic}$ (mm)	2.3-4.7	2.4	2.9	1.2	2.0	3.2	1.2-2.4

Table V : Radii of the central plastic core for several target materials as calculated with Eq.(3). For Be and also for Ti two values of $r_{plastic}$ are given. The smaller one corresponds to the maximum value and the larger one to the minimum value of the yield strength, respectively.

For the considered target materials the radii of plasticity are always larger than $R' \approx 1$ mm. Furthermore, a closer approximation of the radial target temperature distribution, as given in Appendix II by the temperature distribution 3, leads to radii of the central plastic core which are 10% to 30% larger than those listed in Table V.

In the limit that the target parts are thin discs, the circumferential and the radial component of the quasi-static stress are both reduced up to 2/3 of the corresponding ones in cylinders. In addition, the longitudinal stress component can be neglected in thin discs. However, the radius of the central plastic core only decreases to $\sqrt{2/3} \approx 0.82$ of the corresponding value in a cylinder.

Thus, due to a single fast extracted pulse of 400 GeV/c, 10^{13} ppp and a beam diameter of 2 mm, external targets of a diameter similar to the beam waist will get completely overstressed over their whole volume during a time of the order of the characteristic diffusion time. This may lead to a destruction of the target.

3.2.4 Methods to overcome the problem of the quasi-static thermal stress

The two ways to overcome the problem of the quasi-static thermal stress occurring for short burst durations are

i) a blow-up of the beam waist

ii) larger transverse target dimensions

It must be stressed that only the first method offers a fail-safe solution of the problem of quasi-static thermal stress, whereas in the second one uncertainties are still present due to a possible fatigue of the target material.

The maximum stress $\sigma_o \equiv |\sigma_\phi - \sigma_z|$ occurs at the target centre and is typically of the order of [3)]

$$\sigma_o \approx \frac{1}{2} \frac{E \alpha T_o}{1 - \nu} = \frac{3}{4} E \alpha T_o < E \alpha T_o .$$

The values of $E \alpha T_o$ exceed the yield strength of the target materials by a factor of about 10 to 20.

The maximum temperature rise T_o in an external target, obtained along its axis, is proportional to R_b^{-2}, where R_b is the beam radius. Therefore, a blow-up of the beam waist, for which in this report a diameter of 2 mm is assumed, by a factor of 3.2 to 4.5 would reduce the maximum temperature rise T_o by a factor 10 to 20 respectively, which is sufficient to avoid overstressing the target at its centre.

If the requirements of the secondary beam optics permit for operation with fast or fast slow extraction the use of targets of about 1 cm in diameter, then the plastic region in the target centre is surrounded by sufficient elastic material to provide an adequate mechanical strength. In this case, reliable target operation may be possible at the SPS even for fast extracted beams of 400 GeV/c, 10^{13} ppp, and a beam diameter of about 2 mm.

4. Cooling of External Targets

4.1 The cooling of targets by radiation, convection and conduction

External targets which are (i) thin in the direction transverse to the beam i.e. their cross-section is approximately of the same magnitude as

the assumed beam diameter of 2 mm and (ii) mounted in vacuum, can only be cooled by radiation. It will be shown below that the target temperatures obtained with radiation cooling are far too high for a reliable target operation. Therefore, more efficient cooling methods must be applied.

With cooling by forced gas convection, however, moderate temperatures can be attained for thin targets. Nevertheless, this method is bound to the disadvantage that beam windows must be installed to separate the gas of the cooling system from the vacuum of the beam transport system.

In fast extraction it appears to be necessary for reasons of the quasi-static thermal stress to construct targets of transverse dimensions large compared with the diameter of the plastic core around the beam axis, i.e. the target diameter must be of the order of 10 mm. These targets can be cooled either by gas convection or conduction. The latter cooling method has the advantage that in many cases it is more efficient and technically easier than the convection cooling, and in addition, no beam windows are necessary. As in the case of thin targets cooling by radiation only gives unacceptably high target temperatures. Moreover, at the moderate steady-state temperatures obtained in several target materials with convection or conduction cooling, the amount of heat transported by radiation becomes negligible.

4.2 Cooling of targets of thin diameters

4.2.1 The temperature of targets cooled by radiation and convection

The temperature distribution in slender targets develops in the following way. Due to the Gaussian beam profile the deposited energy is non-uniformly distributed along the target radius. Thus, a radial temperature gradient is created which causes the heat to spread uniformly over the target cross-section within a characteristic thermal diffusion time which for slender targets is short compared with the repetition time of the SPS (see section 3.1.1). The variation of the target temperature is considered now only for periods which are long compared with this thermal diffusion time. Therefore, a uniform distribution of the target temperature can be assumed. For the considered processes of radiation and convection,

the heat is carried away only from the target surface. Since the cooling of the target surface proceeds slowly compared with the thermal diffusion which distributes the heat over the target cross-section, the temperature will decrease about uniformly throughout the whole target volume.

Therefore, the following differential equations can be applied which describe the time-dependent change of the uniform temperature T of a target if cooled simultaneously by radiation and convection.

i) During the burst (heating and cooling), $0 \leq t \leq \tau$

$$\frac{Q_o}{\tau} = c_p \rho V \frac{dT}{dt} + \varepsilon \sigma_o S(T^4 - T_m^4) + k_{conv} S(T - T_m) \qquad (4a)$$

ii) After the burst (cooling only), $\tau \leq t \leq \tau_R$

$$0 = c_p \rho V \frac{dT}{dt} + \varepsilon \sigma_o S(T^4 - T_m^4) + k_{conv} S(T - T_m) \qquad (4b)$$

In these equations the following symbols have been used :

τ	:	burst length (s)
τ_R	:	repetition period (s)
t	:	time counted from the beginning of an extraction (s)
T_m	:	temperature of the medium surrounding the target (°K)
T	:	uniform temperature of the target (°K)
Q_o	:	total heat produced in a target by 10^{13} protons of 400 GeV/c (cal)
V	:	target volume (cm^3)
S	:	target surface (cm^2)
R	:	target radius (cm)
σ_o	:	Stefan-Boltzmann's constant ($1.35 \cdot 10^{-12}$ cal $cm^{-2} s^{-1} °K^{-4}$)
ε	:	emissivity of the target surface
k_{conv}	:	convection coefficient (cal cm^{-2} s^{-1} $°C^{-1}$)
c_p	:	specific heat (cal g^{-1} $°C^{-1}$)
ρ	:	mass density (g cm^{-3}).

The solution of these differential equations gives the temperature only implicitly in the form $t = f(T)$. For this type of solution the steady-state temperatures can only be calculated by iterative methods. The steady state is defined so that the temperature variation during a thermal cycle is identical to the one during the preceding cycle.

In the case of cooling either by radiation or convection the steady state can be calculated more easily. Moreover, as shown below moderate temperatures can be obtained for thin targets only with cooling by forced gas convection. Cooling by liquids has not been considered as it is undesirable to surround the target by a medium with a mass density which is of the same order of magnitude as that of the target material. In the case of cooling by forced gas convection the heat loss by radiation can be neglected for most of the considered target materials and therefore the formulae obtained for pure convection cooling can be applied.

4.2.2 Cooling by radiation

To simplify the calculation of the influence of radiation cooling on the target temperature T the following two cases are distinguished:

i) $$\frac{\Delta T}{T_m} \ll 1 \quad \text{for } \Delta T \equiv T - T_m$$

ii) $$\frac{\Delta T}{T_m} \gg 1.$$

In the first case the amount of heat carried away from the target by radiation and convection separately can be easily compared, as $(T^4 - T_m^4)$ can be approximated by $4\, T_m^3\, \Delta T$. Then the differential equation (4a) for $0 \leq t \leq \tau$ becomes

$$\frac{Q_o}{S \cdot \tau} = (4\, \varepsilon\, \sigma_o\, T_m^3 + k_{conv})\, \Delta T + \frac{c_p\, \rho\, V}{S}\, \frac{dT}{dt}\,, \qquad (5a)$$

and the equation (4b) for $\tau \leq t \leq \tau_R$

$$0 = (4\,\varepsilon\,\sigma_o\,T_m^3 + k_{conv})\,\Delta T + \frac{c_p\,\rho\,V}{S}\,\frac{dT}{dt} \quad . \qquad (5b)$$

In the same way as the convection coefficient k_{conv}, which is given below in section 4.2.3 of this chapter for natural and forced convection cooling with several gases, the constant quantity

$$k_{rad} = 4\,\varepsilon\,\sigma_o\,T_m^3$$

determines the amount of heat carried away by radiation per second and °C from a unit target surface of 1 cm^2. Therefore, the ratio k_{rad}/k_{conv} gives a criterion for the relative influence of both processes on the target temperature. In Table VI this ratio is given for a target of 2 mm diameter cooled by radiation and either natural or forced convection with several gases. The table shows that compared with forced convection cooling the amount of heat transported by radiation becomes negligible, in spite of the too optimistic assumption of $\varepsilon = 1$ in this calculation.

For $\Delta T/T_m \gg 1$, the steady-state temperatures for cooling by radiation only are derived from Eqs. (4a) and (4b) under the following assumptions :

i) From $(\Delta T/T_m) \gg 1$ it follows that $T^4 \gg T_m^4$; therefore T_m^4 can be neglected in the Eqs. (4a) and (4b).

ii) In the case of slow extraction the cooling during the burst can be neglected if $\tau \ll \tau_R$.

iii) The characteristic thermal diffusion time t_{diff} is short compared with the repetition time τ_R (see section 3.1.1).

Under these assumptions the solution of the Eqs. (4a) and (4b) at the end of the first burst is

convection cooling by	natural convection		forced convection			
cooling gas	k_{conv} (cal $cm^{-2}s^{-1}\,°C^{-1}$)	$\frac{k_{rad}}{k_{conv}}$ (%)	k_{conv} (cal $cm^{-2}s^{-1}\,°C^{-1}$)	$\frac{k_{rad}}{k_{conv}}$ (%)	k_{conv} (cal $cm^{-2}s^{-1}\,°C^{-1}$)	$\frac{k_{rad}}{k_{conv}}$ (%)
			v = 4m/s		v = 20 m/s	
hydrogen	$41 \cdot 10^{-4}$	3.6	$104 \cdot 10^{-4}$	1.4	$216 \cdot 10^{-4}$	0.7
helium	$28 \cdot 10^{-4}$	5.2	$80 \cdot 10^{-4}$	1.8	$161 \cdot 10^{-4}$	0.9
neon	$13 \cdot 10^{-4}$	11.2	$42 \cdot 10^{-4}$	3.5	$88 \cdot 10^{-4}$	1.7
air	$10 \cdot 10^{-4}$	14.6	$39 \cdot 10^{-4}$	3.8	$82 \cdot 10^{-4}$	1.8
argon	$2 \cdot 10^{-4}$	73.0	$29 \cdot 10^{-4}$	5.6	$55 \cdot 10^{-4}$	2.6

Table VI: Under the assumptions that $\Delta T/T_m \ll 1$, $T_m \approx 300°K$, and $\epsilon = 1$, the coefficients for natural and forced convection k_{conv}, respectively, are compared with the coefficients for cooling by radiation k_{rad}. The values are calculated for a cylindrical target of 2 mm diameter cooled by different gases. For the case of forced convection, gas velocities of v = 4 m/s and 20 m/s are taken.

$$T_{1\tau} = \begin{cases} T_m + \overline{T} & \text{for slow extraction} \\ T_m + T_o & \text{for fast extraction} \end{cases}$$

whereas the corresponding temperature at the end of the first thermal cycle T_{1R} is

$$T_{1R} = \left[(T_m + \overline{T})^{-3} + 3\kappa(\tau_R - \tau) \right]^{-1/3} \quad \text{for either slow or fast extraction}$$

where $\kappa = \dfrac{2\,\varepsilon\,\sigma_o}{c_p\,\rho\,R}$.

In the steady state the corresponding target temperatures T_τ and T_R are calculated from the implicit formulae

$$T_R = \left[(T_R + \overline{T})^{-3} + 3\kappa(\tau_R - \tau) \right]^{-1/3} \quad (6) \text{ for either slow or fast extraction,}$$

and

$$T_\tau = \begin{cases} T_R + \overline{T} & \text{for slow extraction} \\ T_R + T_o & \text{for fast extraction} \end{cases}$$

In Table VII the minimum and maximum temperatures in the steady state are given which would occur in the case of cooling by radiation only for external targets of two diameters and of different materials under the too optimistic assumption that their emissivity is $\varepsilon = 1$. The minimum temperatures T_R at the end of the thermal cycle are the same for slow and fast extraction. The maximum temperature in slow extraction is $T_R + \overline{T}$, where $\overline{T}$ is the adiabatic increase of the uniform target temperature due to one burst. In fast extraction the maximum temperature is $T_R + T_o$, and T_o is the fast temperature rise along the target axis.

For fast extraction, as already seen from Table III, due to the rapid temperature rise along the target axis the heavy materials will melt in this

extraction method		slow or fast	slow	fast	T_{melt} (°C)
target material	target diameter (mm)	T_R (°C)	$T_R + \overline{T}$ (°C)	$T_R + T_o$ (°C)	
Be	2	730	920	1220	1280
	4	700	760	1190	
BeO	2	830	1250	1780	2570
	4	800	940	1750	
B_4C	2	750	1300	1940	2430
	4	760	930	1950	
C +)	2	600	1110	1850	3320 ++)
	4	620	780	1870	
SiC	2	910	1220	1750	2700
	4	880	980	1720	
Al	2	660	730	1440	660
	4	660	660	1400	
Al_2O_3	2	850	1300	1910	2040
	4	890	1070	1950	
Ti	2	880	1670	1890	1670
	4	1000	1450	2010	

+) graphite ++) sublimation point

Table VII : Under the assumptions that $\Delta T/T_m \gg 1$, $T^4 \gg T_m^4$, $\tau \ll \tau_R$, $t_{diff} \ll \tau_R$, and $\varepsilon = 1$ the steady-state temperatures in several target materials are evaluated for cooling by radiation only. The minimum temperature T_R at the end of a thermal cycle and the maximum temperature $T_R + \overline{T}$ for slow extraction as well as the peak temperature $T_R + T_o$ for fast extraction are given for two target diameters.

zone, no matter what type of cooling is applied. Only for BeO, B_4C, C, and SiC target temperatures well below their melting points are obtained for cooling by radiation only.

For slow extraction, the steady-state temperatures in the materials Be, BeO, B_4C, C, SiC, and Al_2O_3 are rather high but below the melting point T_{melt}. For Al and Ti the melting point is reached or exceeded by the uniform temperatures $T_R + \overline{T}$ except for the titanium target of 4 mm diameter.

Table VII shows that for light target materials the temperature T_R reached at the end of a repetition period for a target diameter of 2 mm is somewhat larger than for a diameter of 4 mm, whereas for heavy target materials this order is inverted. This results from the fact that for light target materials, the term with $(T_R + \overline{T})^{-3}$ of Eq. (6) contributes significantly, whereas for heavy materials this term can be neglected compared with $3\,\kappa(\tau_R - \tau)$. In this latter case the temperature increases proportional with $R^{1/3}$ and therefore a higher temperature T_R is reached in targets of larger diameters.

The true emissivity of a surface strongly depends on the material as well as on the state of the surface. Nevertheless, for all materials given in Table VII an emissivity of $\varepsilon = 1$ is applied, which leads to the lowest temperature that can be obtained by radiation cooling only. If, for instance, the emissivity is $\varepsilon = 0.5$ the temperature T_R augments by about 26% and correspondingly also the maximum temperatures $T_R + \overline{T}$, and $T_R + T_o$ will increase. Even if the steady-state temperatures obtained for $\varepsilon = 1$ do not reach the melting point, they are too high for reliable target operation. Therefore, a cooling mechanism must be applied which at low surface temperatures is more efficient than radiation cooling.

4.2.3 Cooling by convection

The formulae used for the calculation of the convection coefficients k_{conv} for thin cylinders [10, 11, 12] are given in Appendix III.

The target cylinder is always placed horizontally in the cooling medium and in case of forced convection a gas stream perpendicular to the cylinder axis is assumed. If, for comparison a gas flow of the same velocity but parallel to this axis is applied, the coefficient for forced convection would be reduced by about 50% as shown in Fig. 4 [10].

Table VIII shows the calculated values of the coefficients for natural and forced convection for the gases hydrogen, helium, neon, air and argon and for target diameters of 2 mm and 4 mm respectively. In the case of forced convection, gas speeds of 4 m/s and 20 m/s are assumed.

The forced convection coefficient will increase for a given gas by a factor between 2 and 3, depending on Reynolds number, if the velocity of the gas stream is augmented by a factor of 10. The highest convection coefficients are obtained for hydrogen followed by helium, neon, air and argon.

By a target construction with fins in the longitudinal direction, the total surface used for cooling can be augmented without a significant increase of the deposited beam energy, if the requirements for the beam optics permit an extension of the target size.

Table VIII shows for the gases H_2, He,Ne and air that already in the case of a low gas speed of 4 m/s the coefficients for forced convection exceed those for natural convection by approximately a factor of 3. Correspondingly, the target temperatures achieved by forced convection cooling are much lower than those for natural convection.

Thus, for slender external targets at the SPS, where on the one hand a large amount of energy deposited by the beam has to be carried away and on the other hand the occurring temperatures must be kept well below the melting points for reliable operation, cooling by forced convection must be applied.

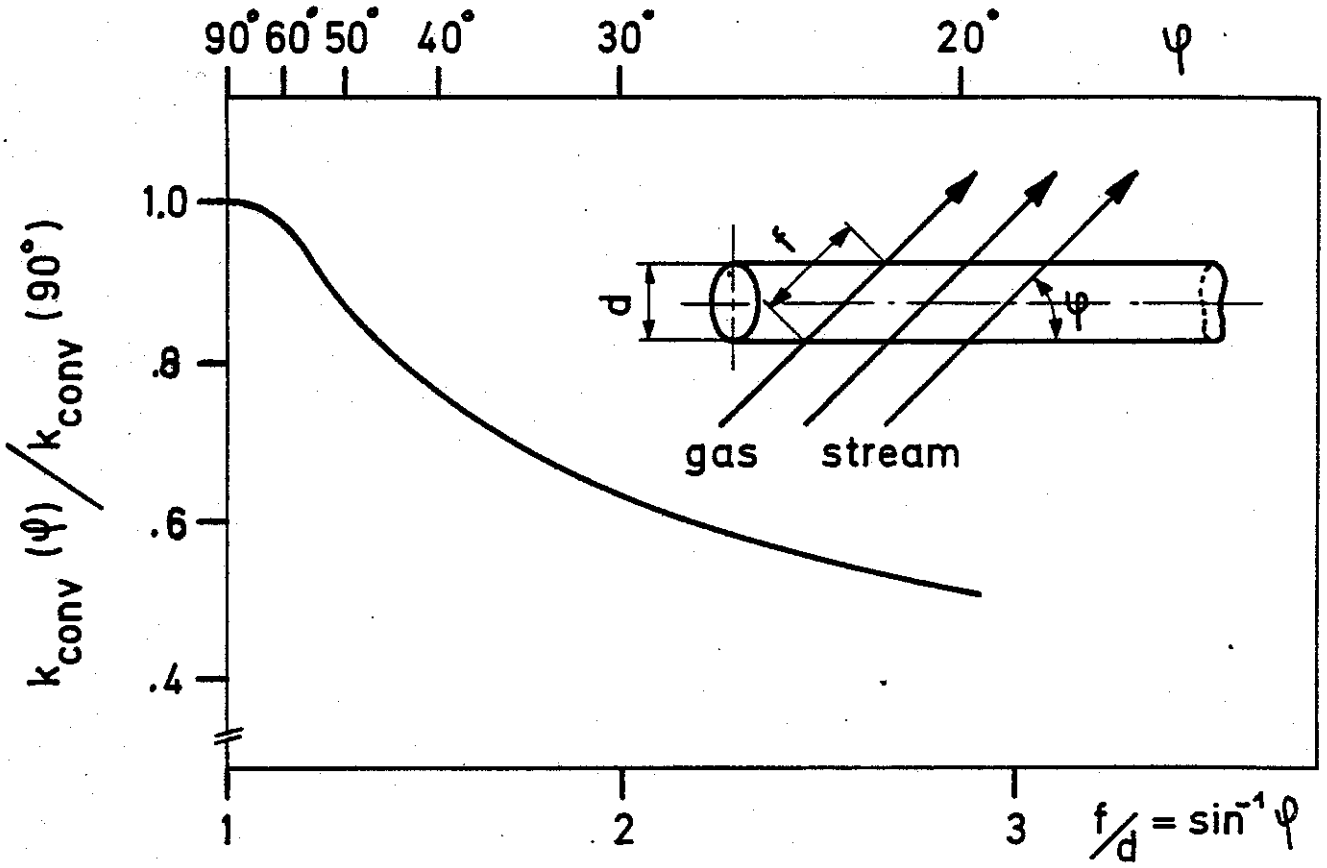

Fig. 4 Angular dependence of the coefficient for forced gas convection cooling k_{conv} normalized to the value obtained for a perpendicular gas stream.

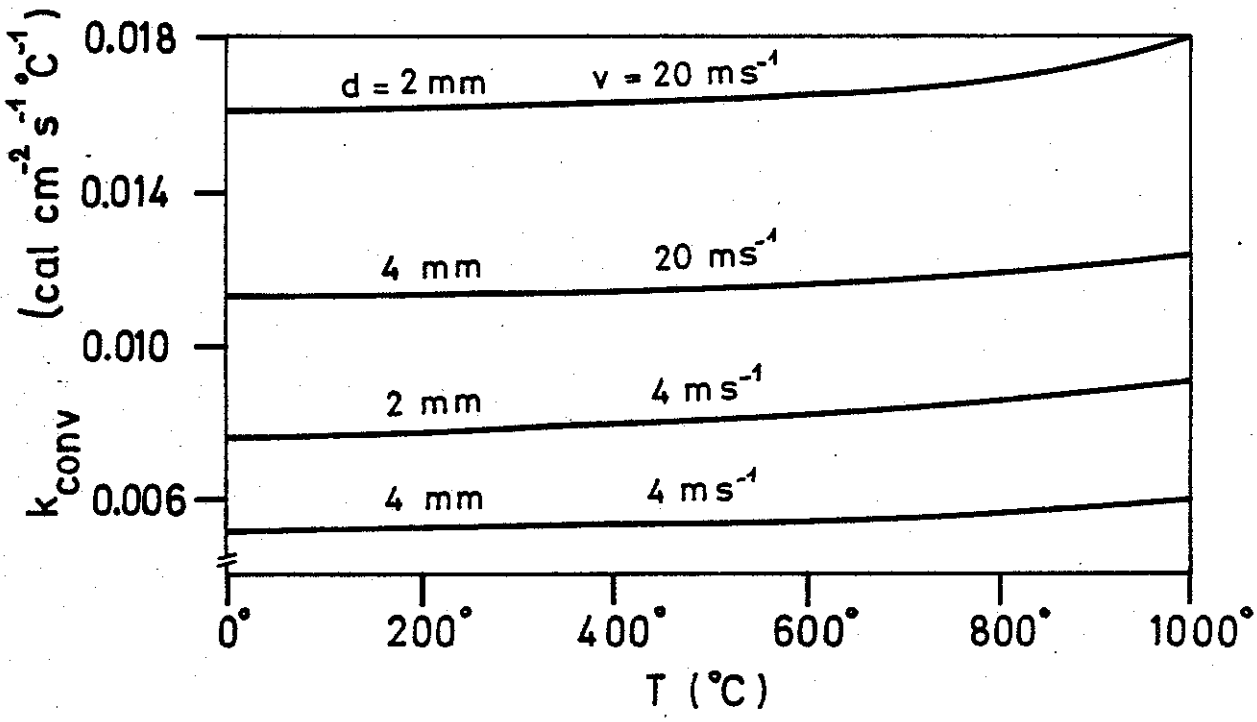

Fig. 5 Forced convection coefficients k_{conv} in helium as a function of the surface temperature T of the cylindrical target for two diameters d and two gas velocities v.

target diameter (mm)	coefficients for natural convection (cal cm^{-2} s^{-1} $°C^{-1}$)					gas velocity (m/s)	coefficients for forced convection (cal cm^{-2} s^{-1} $°C^{-1}$)				
	H_2	He	Ne	Air	Ar		H_2	He	Ne	Air	Ar
2	$41 \cdot 10^{-4}$	$28 \cdot 10^{-4}$	$13 \cdot 10^{-4}$	$10 \cdot 10^{-4}$	$2 \cdot 10^{-4}$	4	$104 \cdot 10^{-4}$	$80 \cdot 10^{-4}$	$42 \cdot 10^{-2}$	$39 \cdot 10^{-2}$	$26 \cdot 10^{-4}$
						20	$216 \cdot 10^{-4}$	$161 \cdot 10^{-4}$	$88 \cdot 10^{-4}$	$82 \cdot 10^{-4}$	$55 \cdot 10^{-4}$
4	$26 \cdot 10^{-4}$	$20 \cdot 10^{-4}$	$9 \cdot 10^{-4}$	$7 \cdot 10^{-4}$	$0.3 \cdot 10^{-4}$	4	$70 \cdot 10^{-4}$	$53 \cdot 10^{-4}$	$29 \cdot 10^{-4}$	$27 \cdot 10^{-4}$	$18 \cdot 10^{-4}$
						20	$149 \cdot 10^{-4}$	$112 \cdot 10^{-4}$	$61 \cdot 10^{-4}$	$57 \cdot 10^{-4}$	$38 \cdot 10^{-4}$

Table VIII : Coefficients for natural and forced convection for cylindrical targets of 2 mm and 4 mm diameter, respectively, cooled with the gases H_2, He, Ne, air, and Ar. The mean gas temperature is $T_m = 25°C$. The values are given for targets which are mounted horizontally, and in the case of forced convection a gas stream perpendicular to the cylinder axis is assumed with a velocity v = 4 m/s and 20 m/s, respectively.

The influence of the surface temperature of the target cylinder and of the temperature dependence of the gas constants on the coefficients for natural and forced convection has been studied. Although the dimensionless quantities like Prandtl, Grashof, Reynolds and Nusselt number (see Appendix III) are varying with temperature, the convection coefficients are nearly temperature independent as demonstrated in Fig. 5 for the case of forced convection cooling with a helium gas stream of two velocities for two target diameters.

In principle, one would like to choose hydrogen as a cooling medium for it offers the highest convection coefficients, but this gas requires special safety provisions. By using helium this disadvantage is avoided, and for a given gas speed its forced convection coefficient is still about 75% of the one for hydrogen. Moreover, for any velocity of a helium gas stream, which is twice as high as the corresponding velocity for a hydrogen gas stream, the values of the forced convection coefficients for both gases will become equal.

4.3 Cooling of targets of large transverse dimension

4.3.1 Cooling by conduction

The following calculations are limited to targets made of plates with a rectangular cross-section. The thickness of a target plate is supposed to be small compared with its width. For operation in slow extraction the plate thickness can be made comparable with the beam diameter of 2 mm. Targets constructed for fast extracted beams must have a thickness of about 1 cm, in order to avoid failure due to the quasi-static thermal stress. In addition, these latter targets will consist longitudinally of several parts with lengths taken from Table IV, in order to decrease the longitudinal component of the dynamic thermal stress.

For plate targets cooling by conduction only is assumed here. As shown in Fig. 6 only the central part of the target is heated directly by the proton beam. The produced heat is transported via conduction across the plate towards the cooled side-faces. The target can be placed directly

into the vacuum system of the beam transport lines. Therefore, this scheme has the advantage that corrosion of the heated target is prevented.

The heat transport by thermal conduction only can be easily calculated for the approximation that the pulsed heating of the target is replaced by a continuous heating. In addition, it is assumed that the heat is produced by a vertical plane source which is situated in the centre of the plate as shown schematically in Fig. 6. The side-faces of the plate are kept at a constant temperature T_{surf} by a suitable cooling. The temperature T(x) in the x - direction of the plate is given by

$$T(x) = \frac{q\ b}{2\ \lambda\ S_c}\left(1 - \frac{|x|}{b}\right) + T_{surf} \qquad (7)$$

where

q	:	continuous heat flow emitted from the plane source (cal/s)
d	:	plate thickness (cm)
ℓ_{total}	:	total length of the target (cm)
S_c	:	area of the heat source, $d \cdot \ell_{total}$ (cm^2)
λ	:	thermal conductivity (cal $cm^{-1}s^{-1}°C^{-1}$)

For a plate target made from Be with b = 10 cm, d = 1 cm and T_{surf} = 25° C the temperature obtained from Eq. (7) at x = 0 is T(o) = 49°C. Although the assumption given above simplifies the true heat transfer considerably, this result agrees well with the corresponding steady-state temperature of $T_R = (46 \pm 2)$ °C at the end of a thermal cycle, calculated with a Monte Carlo programme which simulates the heat diffusion in this Be-plate if irradiated by a pulsed proton beam with a burst length of infinitesimal duration [13]. The maximum temperature T_τ reached at the end of a fast extracted pulse is, of course, obtained if the fast temperature rise T_o is added to the temperatures T(o) and T_R, respectively, given above.

Cooling by conduction can be applied for target operation in slow extracted beams in those cases where the requirements on secondary beam

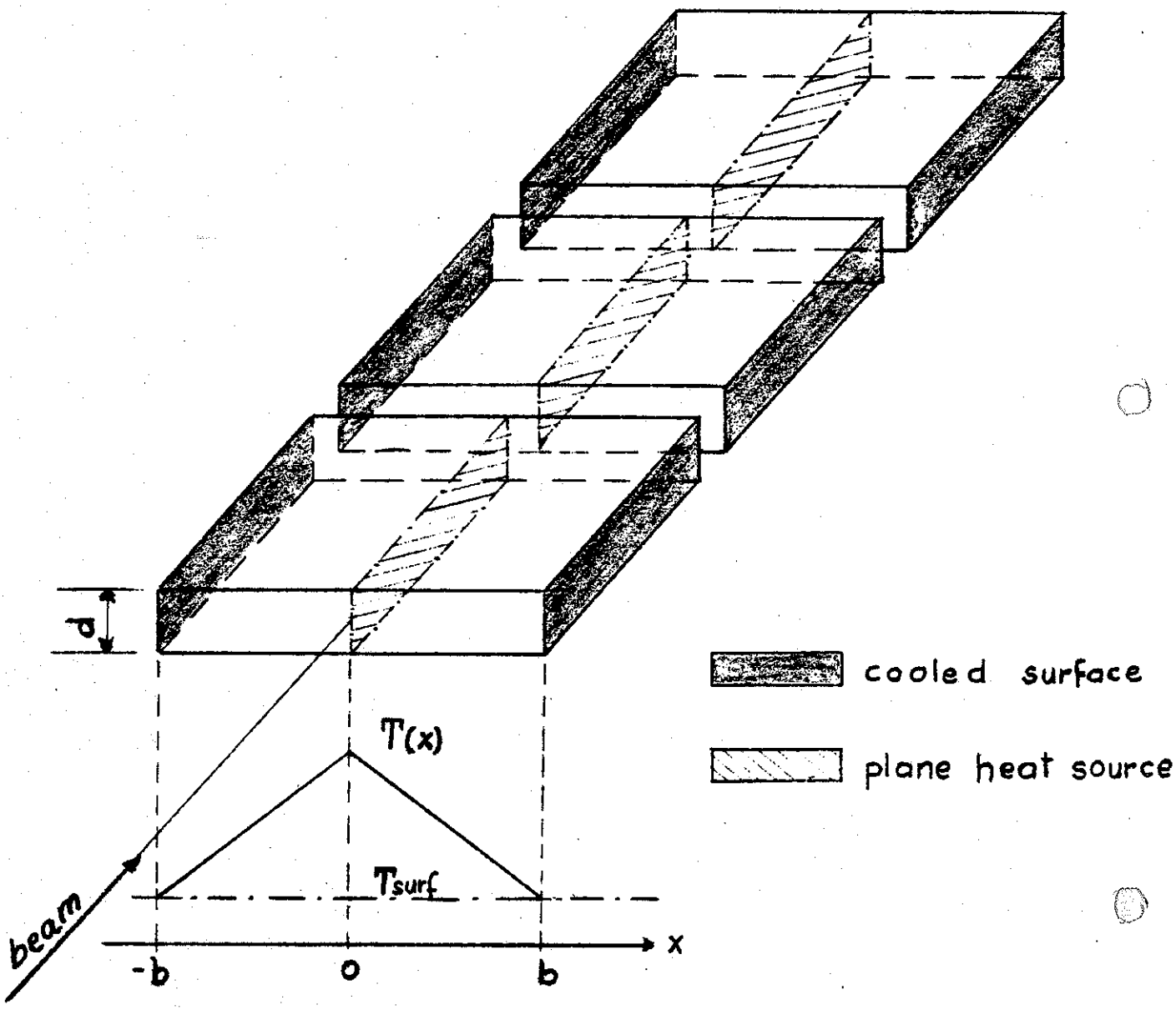

Fig. 6 : A plate target longitudinally divided in e.g. three parts. It is assumed that each target part is heated along its central vertical plane by a constant plane source and cooled only at both side-faces to a temperature T_{surf}. The transverse temperature distribution represented by Eq. (7) is also shown.

optics permit the use of plate-like targets with a thickness comparable with the beam diameter in one transverse direction.

For plate-like targets made e.g. from beryllium with a thickness of d = 0.2 cm, a width of 2b = 10 cm, and T_{surf} = 25°C, the maximum steady-state temperature is T(o) = 70°C if again a continuous heating by a plane source is assumed.

A disadvantage of these plate-like targets is a possible increase of the size of the source of the secondary beam. This increase can be caused by the additional interactions of protons, which are contained in the beam fringes and hit the lateral target material on both sides of the central target region. Thin plate-like targets, however, can be made to approach the preferable pencil-like shape if the plate material which is hit by the protons contained in the possible beam fringes is reduced considerably. This can be achieved with e.g. two grooves cut symmetrically on both sides of the target centre as shown schematically below.

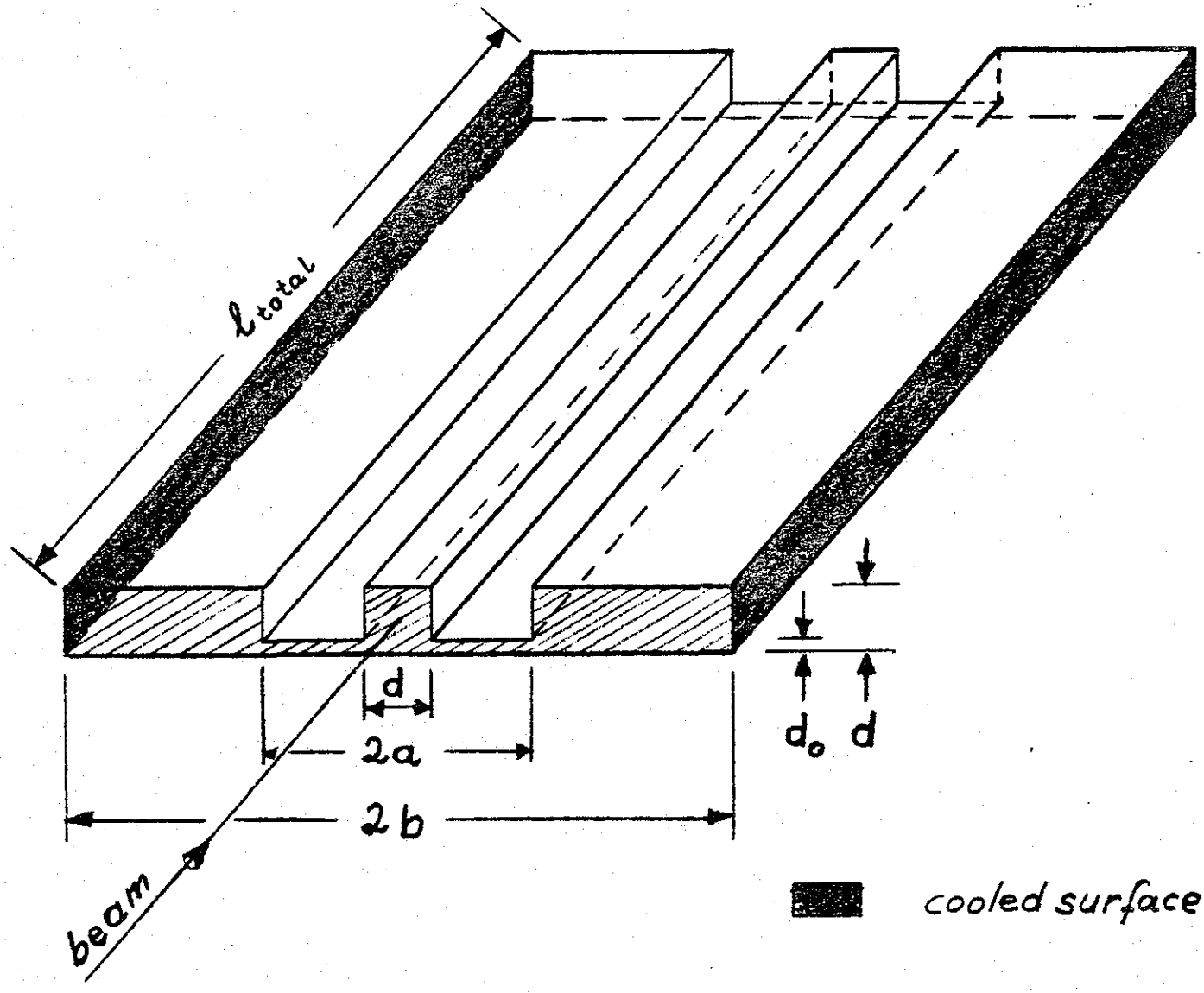

Again, the assumption of a Gaussian beam shape is made which permits to estimate the contribution of the interactions produced by primary protons with a distance from the beam centre larger than e.g. the beam radius (Appendix I).

For the target of such a shape with a thickness of d = 0.2 cm which is reduced to d_o = 0.04 cm in the grooves on both sides of the target centre, less than 1% of the interacting protons will be absorbed in the material extending from the central part. In this way, the influence of a possible beam halo on the size of the source of the secondary beam may become negligible.

Assuming again a continuous heating of the target by a vertical plane source, the maximum temperature occurring at the target centre is given by

$$T(o) = \frac{q\ b}{2\ \lambda\ S_c}\left[1 - \frac{a\ d}{b\ d_o}\right] + T_{surf}\ , \qquad (8)$$

where a, b, d and d_o are indicated in the above sketch.

For a target made from beryllium with d = 0.2 cm, d_o = 0.04 cm, a = 0.6 cm which corresponds to a distance of three beam diameters, b = 5 cm, and T_{surf} = 25°C the maximum steady-state temperature is T(o) = 90° C. This temperature is still less than 10% of the melting point of beryllium and the corresponding yield strength of this material is approximately the same as at room temperature. Therefore, it appears advantageous to use such plate-like targets for slow extracted beams.

4.3.2 Comparison of cooling by conduction and convection

As discussed before, cylindrical targets must be cooled by forced convection, whereas a plate target can be cooled by conduction. To compare these two cooling mechanisms the condition is considered under which the temperatures at the target centre are identical for (i) a cylindrical target of diameter d and (ii) a plate target with a cross-

sectional area of 2bd in the plane transverse to the beam. This condition is given by

$$k_{conv} \approx \frac{2}{\pi} \frac{\lambda}{b} \qquad (8)$$

In Table IX, the distance b is given for several target materials to compare the efficiency of both cooling mechanisms. For the diameter of the cylindrical target as well as for the plate thickness a value of d = 0.2 cm is assumed. The convection coefficient of $k_{conv} = 161 \cdot 10^{-4}$ cal $cm^{-2}s^{-1}°C^{-1}$ is calculated for helium with a gas stream of 20 m/s. Therefore, the above relation can simply be written as $b \approx 40\ \lambda$, where λ is given in units of (cal $cm^{-1}s^{-1}°C^{-1}$) and b in (cm). For the case of larger values of d the magnitude of the forced convection coefficient will decrease and therefore the distance b will even be enlarged.

target material	b (cm)
Be	14.4
BeO	22.8
B_4C	3.0
C	4.4
SiC	8.4
Al	22.0
Ti	1.9

Table IX : Comparison of convection and conduction cooling. The distance b defined with Eq. (8) is given for several target materials.

Table IX shows that the heat transport by conduction is in most cases more efficient than heat transfer by convection, as in general, the target dimensions transverse to the beam direction will be small compared with the values of b.

Nevertheless, as shown below, for some of the target constructions pro-

posed for the operation in fast extraction, conduction cooling cannot be applied and therefore cooling by forced convection must be chosen.

5. External targets in slow and fast extracted beams

5.1 The windows for the target enclosure

5.1.1 Beam windows in slow extracted beams

For the cooling of targets by convection, beam windows are necessary to separate the gas system from the vacuum system. In slow extraction, if burst lengths $\tau \gtrsim 50$ ms are assumed, the beam windows are not affected by quasi-static or dynamic thermal stress.

The maximum temperature increase in an aluminium foil is about 80°C for a burst duration of 50 ms and 10°C for a burst length of 700 ms. These values are reached at the end of a slow extracted proton pulse of 400 GeV/c, 10^{13}ppp, and a beam diameter of 2 mm. However, the temperatures given here are rather pessimistic, since it has been assumed that the distribution of the energy deposition density in an Al-target is also valid for a thin Al-window. The construction of beam windows for slow extracted beams of duration longer than about 50 ms will introduce no problems due to the rather small temperature rise.

5.1.2 Beam windows in fast extracted beams

For several target constructions proposed below for fast extraction, cooling by forced gas convection must be applied. Due to the small burst length of $\tau \leq 23$ μs the beam windows are affected by quasi-static and dynamic thermal stress. In addition, these vacuum windows are already prestressed by a pressure of one atmosphere. These problems remain to be studied.

5.2. Steady-state temperatures of solid cylindrical targets cooled by forced gas convection

5.2.1 Steady-state temperatures in slow extraction

The formulae which describes the temperature cycling for the first thermal cycles and for the steady state are developed in Appendix IV.

Figure 7 shows this time-dependent variation of temperature for a beryllium target of 2 mm diameter cooled with a constant helium flow of 20 m/s. For the steady-state cycling which is already reached after a few machine cycles, the temperature at the beginning of a repetition period is

$$T_R = T_\infty \frac{1 - e^{\zeta\tau}}{1 - e^{\zeta\tau_R}} + T_m \,, \tag{9}$$

where $$\zeta = \frac{2\, k_{conv}}{c_p\, \rho\, R} \,, \quad T_\infty = \frac{Q_o}{\tau\, S\, k_{conv}}$$

and T_m is the temperature of the incoming gas ($\approx 25^\circ C$).
During the burst the temperature rises to its maximum value

$$T_\tau = (T_R - T_m)\, e^{\zeta(\tau_R - \tau)} + T_m \tag{10}$$

obtained at the end of the burst. Thereafter, the temperature decreases exponentially and again reaches its initial value T_R at the end of the thermal cycle.

Figure 8 demonstrates that convection cooling is a rather slow process since the minimum and maximum steady-state temperatures T_R and T_τ respectively, plotted as a function of the burst length τ do not change drastically for $0 < \tau \leq 1s$.

In Table X the maximum and minimum target temperatures T_τ and T_R for slow extraction are given. The values are calculated for forced convection cooling with the gases H_2, He, Ne, air and Ar for two different velocities and for the target diameters of 2 mm and 4 mm.

5.2.2 Steady-state temperatures in fast extraction

The steady-state temperature at the end of a thermal cycle derived in Appendix IV is given by

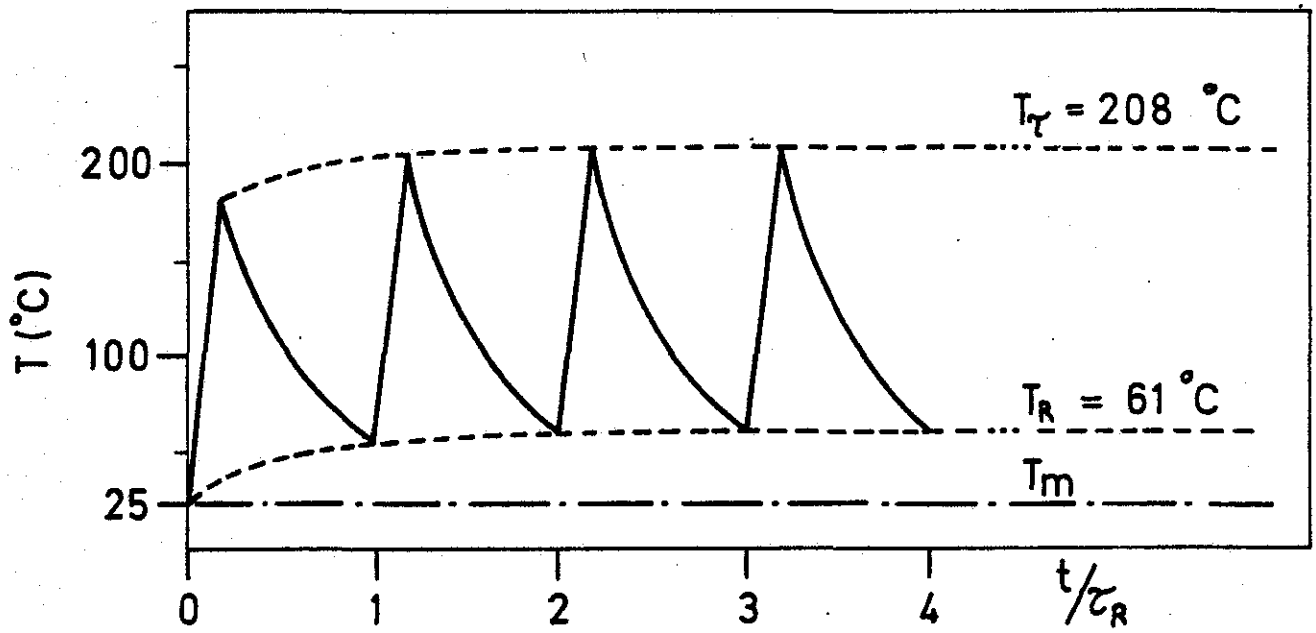

Fig. 7 The variation of the temperature T at the target surface during the first thermal cycles is shown for a Be-target of 2 mm diameter cooled by forced convection with helium. For the gas stream a velocity of 20 m/s and a temperature of T_m = 25°C are assumed. The steady-state temperatures T_τ and T_R are already reached after a few machine cycles.

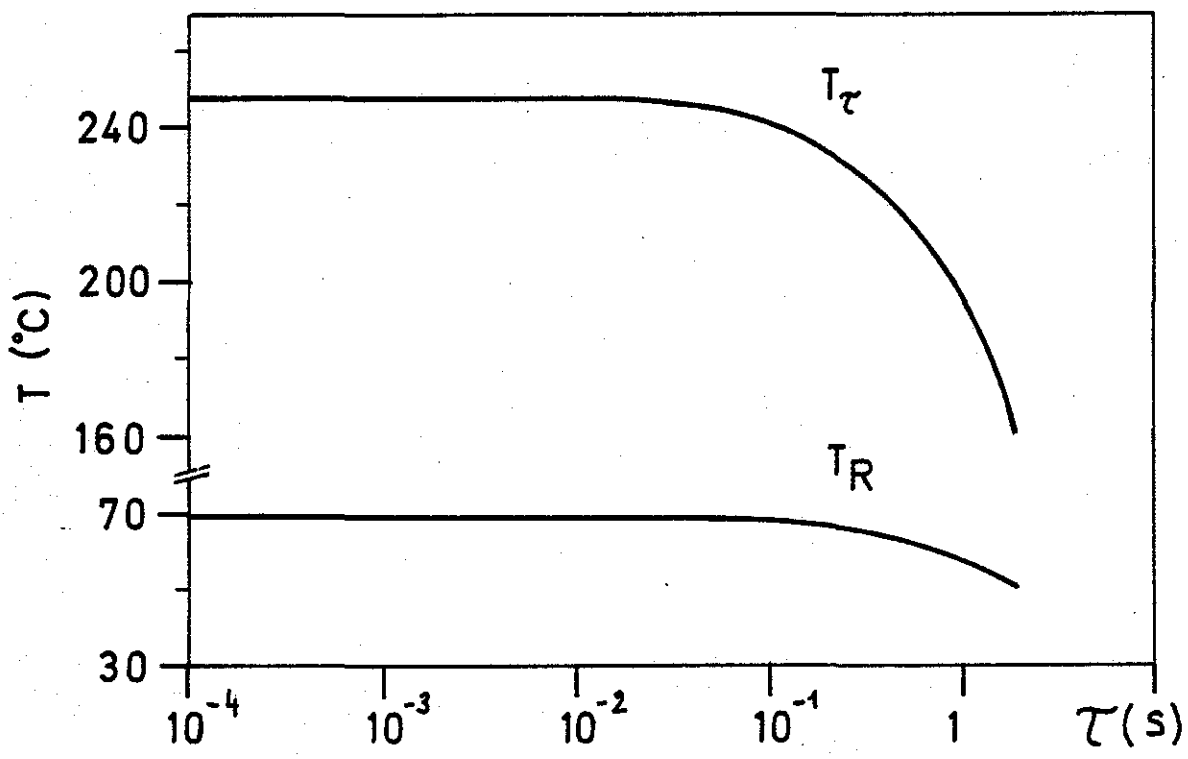

Fig. 8 Steady-state temperatures T_τ and T_R at the target surface as a function of the burst length τ for a Be-target of 2 mm diameter cooled by forced gas convection with helium. For the gas stream a velocity of 20 m/s and a temperature T_m = 25°C are assumed.

gas	gas velocity	target diameter	steady-state temperatures for targets in slow extracted beams									
			T_R (°C)					T_τ (°C)				
	m/s	mm	Be	BeO	B_4C	C +)	SiC	Be	BeO	B_4C	C +)	SiC
H_2	4	2	110	160	110	50	220	260	480	520	400	460
		4	150	270	220	110	350	200	400	380	250	450
	20	2	40	50	40	30	80	180	350	400	320	310
		4	70	110	90	40	160	120	240	250	180	260
He	4	2	150	230	170	70	310	300	550	590	440	550
		4	200	370	310	160	470	250	500	470	300	570
	20	2	60	80	50	30	120	210	390	440	250	360
		4	90	160	130	60	210	150	300	290	200	310
Ne	4	2	310	530	430	200	660	470	850	850	580	900
		4	360	700	610	310	880	410	830	770	460	970
	20	2	130	200	150	60	270	280	520	560	320	510
		4	170	320	260	130	410	220	440	420	280	510
air	4	2	340	580	480	220	710	490	900	900	600	960
		4	380	760	650	340	950	440	890	810	480	1050
	20	2	140	220	160	70	300	300	540	580	430	540
		4	180	340	280	140	440	240	470	450	290	540
Ar	4	2	530	930	790	390	1120	690	1250	1210	780	1360
		4	580	1160	1010	530	1430	630	1280	1170	680	1540
	20	2	230	380	300	130	480	380	700	720	510	720
		4	270	530	450	230	670	320	660	610	380	770

Table X : The steady-state temperatures of external targets of 2 mm and 4 mm diameter in slow extracted beams are given for forced convection cooling with several gases of two different velocities. T_R is the minimum temperature obtained at the end of a thermal cycle (τ_R = 4.77s), and T_τ the maximum temperature reached at the end of a burst (τ = 0.7s). For the incoming gas stream a mean temperature of T_m = 25°C is assumed.

$$T_R = \frac{\overline{T}}{e^{\zeta\tau_R} - 1} + T_m \,, \qquad (11)$$

where $\overline{T}$ is the difference between the uniform target temperatures obtained at the time $t \approx t_{diff}$ and at the end of the preceding thermal cycle. $\overline{T}$ depends on the target diameter and was calculated in chapter 3 by integrating the energy deposition density over the target cross-section.

It has been shown in section 3.1.1 that for fast extraction the burst duration τ is small compared with the characteristic thermal diffusion time t_{diff}. Therefore, in the beginning of each thermal cycle, a radial temperature gradient is superimposed on the uniform temperature distribution achieved by heat diffusion during the preceding period. This leads to the peak temperature $T_R + T_o$ which is obtained along the target axis at the end of a burst.

In Table XI the steady-state temperature T_R and the peak temperature $T_R + T_o$ are given for forced convection cooling with the gases H_2, He, Ne, air and Ar at gas velocities of 4 m/s and 20 m/s and for target diameters of 2 mm and 10 mm.

Although targets of a cross-section comparable to the beam diameter will get completely overstressed in fast extraction as shown in section 3.2.3, the steady-state temperatures for a target diameter of 2 mm are nevertheless given, so that they can be scaled down in the case of a reduced proton intensity.

5.3 Special target constructions for fast extracted beams

5.3.1 A target made from discs

It has been shown in section 3.2.2 that the dynamic thermal stress becomes negligible, if the target of a total length corresponding to one interaction mean-free path, is cut into parts each of a length of ℓ_{10} given in Table IV.

gas	gas velocity	target diameter	steady-state temperatures for targets in fast extracted beams									
			T_R (°C)					$T_R + T_o$ (°C)				
	m/s	mm	Be	BeO	B_4C	C [+)]	SiC	Be	BeO	B_4C	C [+)]	SiC
H_2	4	2	120	180	130	50	260	610	1130	1320	1300	1100
		10	150	330	280	150	380	640	1280	1470	1400	1220
	20	2	50	60	40	30	90	540	1010	1230	1280	980
		10	80	160	140	80	190	570	1110	1330	1330	1030
He	4	2	170	270	200	80	360	660	1220	1390	1330	1200
		10	190	430	360	200	490	680	1380	1550	1450	1330
	20	2	70	90	60	30	140	560	1040	1250	1280	980
		10	100	220	180	100	250	590	1170	1370	1350	1090
Ne	4	2	370	620	510	230	780	860	1570	1700	1480	1620
		10	340	810	680	360	910	830	1760	1870	1610	1750
	20	2	150	230	170	70	320	640	1180	1360	1320	1160
		10	170	400	330	180	450	660	1350	1520	1430	1290
air	4	2	400	670	560	260	840	890	1620	1720	1510	1680
		10	360	850	720	390	960	850	1800	1910	1640	1800
	20	2	170	280	190	80	350	660	1210	1380	1330	1190
		10	180	420	350	190	470	670	1370	1540	1440	1310
Ar	4	2	630	1080	930	450	1320	1120	2030	2120	1700	2160
		10	540	1310	1110	590	1480	1080	2260	2300	1840	2320
	20	2	270	440	350	150	570	760	1390	1540	1400	1410
		10	270	630	530	290	710	760	1580	1720	1540	1550

Table XI : The steady-state temperatures of external targets of 2 mm and 10 mm diameter in fast extracted beams are given for cooling by forced convection with several gases of two different velocities. T_R is the minimum temperature obtained at end of a thermal cycle (τ_R = 4.77s), and $T_R + T_o$ the peak temperature reached along the target axis at the end of a burst (τ = 23 µs). For the incoming gas stream a mean temperature of $T_m = 25^oC$ is assumed.

If, in addition, the target diameter is about 1 cm, then the plastic core around the target axis created by the quasi-static thermal stress is surrounded by sufficient elastic material to provide an adequate mechanical strength. Under these conditions it may be expected that the target can be reliably operated even for fast extracted beams of 400 GeV/c, 10^{13} ppp, and a beam diameter of 2 mm. Nevertheless, it cannot be excluded that the repeated overstressing of the region around the target axis will reduce the target lifetime to an unacceptably short duration. This latter point will perhaps be answered by experience at NAL before the SPS comes into operation.

The target can be cooled with forced gas convection. The steady-state temperatures occurring in the targets are given in Table XI of the previous section for a target diameter of 1 cm.

5.3.2 Granular target material

One possibility of reducing the dynamic thermal stress in external targets for fast extracted beams is to construct targets consisting of granular material. This offers the following advantages :

i) The dynamic stress produced by thermal shock can be neglected due to small granule diameters.

ii) The excess of the quasi-static thermal stress above the yield strength can only affect an individual granule and will not change the overall structure of the target material.

However, this granular material must be enclosed in a container which provides sufficient mechanical rigidity to withstand the flow of the cooling gas around it and avoids contamination of the gas cooling system by spilled target material. The problem for this granular target is to find reliable container windows close to the target material. This is particularly difficult for the exit window as it is traversed by the secondary particles as well as by the non-absorbed primary protons.

A disadvantage of this target construction is that the thermal conductivity λ is reduced in granular materials, and therefore the characteristic thermal diffusion time which is proportional to λ^{-1} increases correspondingly. Nevertheless, if the thermal conductivity is not decreased to less than 10% of the value for the massive material, then the time needed to dissipate the heat uniformly over the whole target volume is of the order of 100 ms to 600 ms which is still short compared to the duration of about 5s of a thermal cycle. Thus, even for a granular target the steady-state temperature evaluated for massive materials may be applied approximately.

It will be necessary to chose a target diameter of about one centimetre to neglect the thermal stress problem in the container wall.

Graphite which has a high sublimation point may be used as a granular target material. The graphite must, of course, be kept in an inert atmosphere.

5.3.3 A carbon fibre target rotating with a low frequency

The production of carbon fibres, which is a rather new branch of technology, offers a material of high tensile strength and high stiffness (Young's modulus), but low specific gravity. For two representative types of carbon fibres values of these material properties are given in Table XII. In addition, the sublimation point for carbon is about 3300°C in an inert atmosphere.

	diameter (μ)	ρ ($g\ cm^{-3}$)	E ($kp\ mm^{-2}$)	α ($°C^{-1}$)	$\sigma_{tensile}$ ($kp\ mm^{-2}$)
carbon fibre I	8.0	1.86	$38 \cdot 10^2$	$-1.7\ 10^{-6}$	173
Carbon fibre II	8.5	1.74	$25 \cdot 10^2$	$-0.8\ 10^{-6}$	241

Table XII : The specific gravity ρ , Young's modulus E, the linear coefficient of thermal expansion α , and the tensile strength $\sigma_{tensile}$ are given at room temperature for two types of carbon fibres [14].

If the quasi-static thermal stress in a single carbon fibre is considered, the radial and circumferential components vanish since due to the very small diameter a temperature gradient can only be produced along a filament. Thus, by placing the fibres parallel to the beam direction the temperatures along a filament will be rather uniform and also the longitudinal stress component can be neglected.

It is assumed that due to the filamenteous structure of the target material longitudinal stress waves cannot be transmitted.

A target, where the material hit by the beam consists of carbon fibres can be constructed in the following way : Carbon fibres are available in the form of tows and tapes containing about 10.000 individual filaments. In the case of the tape the filaments are held parallel with carbon fibre yarn weft. Using a cylinder with a central axis, the carbon tape is rolled several hundred times around the cylinder to produce a carbon layer of several millimetres thickness. A modified construction is to attach carbon fibre tows at the cylinder surface. In both cases the orientation of the filaments will be parallel to the beam axis. The assembled target is shown schematically below. The proton beam incident parallel to the cylinder axis hits the carbon fibres situated on the periphery of the target.

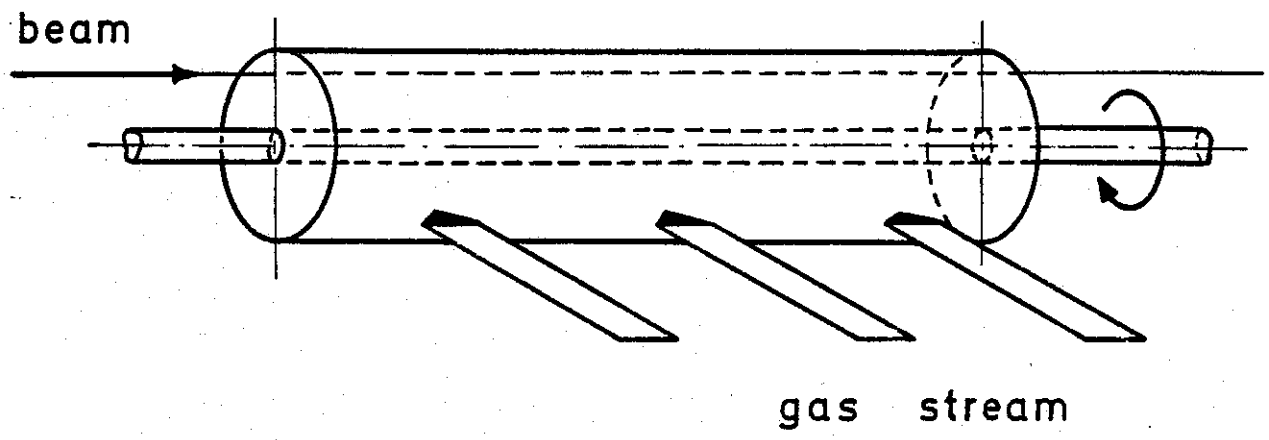

The heated carbon fibres must be kept in inert atmospheres. Therefore, the target will be placed inside a tank filled, for instance, with helium gas. To augment the time in which the same target spot is hit twice by the beam, the target cylinder is made to rotate around its longitudinal axis. For a rotation frequency of about 100 revolutions per minute and a cylinder diameter of 10 cm, about every hundredth pulse will fall onto the same target spot.

By the rotation of the target cylinder in a container filled with helium gas, the heated fibres are cooled by forced convection. The rotation can be produced by either a driving axle or a gas stream blowing eccentrically onto the target, perpendicular to its axis.

5.3.4 A target rotating with a high frequency

For an external target heated by a fast or a fast slow extracted proton pulse of Gaussian beam profile, the approximate range of the linearly decreasing temperature is given by the beam radius, as shown in Fig. 2. Therefore, the magnitude of the temperature gradient is defined by the maximum temperature rise T_o reached along the beam axis (see Table III). The amplitudes of the quasi-static and the dynamic thermal stress are both dependent on T_o. By the use of a rapidly rotating cylinder which is hit by the proton beam near its periphery, the maximum temperature rise T_o and therefore the values of the thermal stresses can be reduced. The target can be cooled efficiently by its rotation in a helium atmosphere.

However, due to the centrifugal forces, stress is created in a rotating cylinder. The maximum stress in a solid cylinder of radius R and rotation frequency ν_{rot} occurs at the axis of rotation [3] and is

$$\sigma_{rot} = \frac{3 + \nu}{8} \rho \, (2\pi\nu_{rot} \, R)^2 . \qquad (12)$$

For a rotating cylinder with a central hole and a wall which is thin compared with the diameter of the cylinder, the maximum stress σ_{rot} is

increased by approximately a factor of 2.4 [3].

A rotating target constructed for operation in fast slow extracted beams with spill durations down to a few milliseconds will cause no serious technical problem. A rotation frequency of about 2000 revolutions per minute will be necessary for a cylinder of 20 cm diameter to reduce the temperature rise T_o by a factor of 20. Therefore, the quasi-static thermal stress will be decreased to values below the yield strength for the target materials listed in Table V. The corresponding mechanical stress produced in the cylinder due to its rotation will be negligible, (less than 1 $^{o}/_{oo}$ of the yield strength for the considered target materials).

However, for a target constructed for the operation in fast extracted beams the rotation frequency must be extremely high in order to reduce sufficiently the temperature rise which is reached at the end of a pulse of 23 μs duration. In Figure 9 the maximum stress produced in a solid titanium cylinder by its rotation is shown as a function of the reduced temperature rise T.

A separate abscissa also gives the corresponding rotation frequencies ν_{rot} for a cylinder of 20 cm diameter. The temperature dependent yield strength is shown for comparison for pure titanium and several of its alloys. It can be seen that there is a considerable temperature range for several titanium alloys where the maximum values of the stress σ_{rot} are 10 % to 20 % of the yield strength. Nevertheless, the required rotation frequencies of about $2 \cdot 10^4$ revolutions per minute will be too high for a reliable target design.

6. Conclusion

In this report the thermal problems have been studied which occur for external targets heated by slow and fast extracted beams of 400 GeV/c, 10^{13} ppp, and a beam diameter of 2 mm. The reported values of the expected target temperatures and thermal stresses are calculated with a

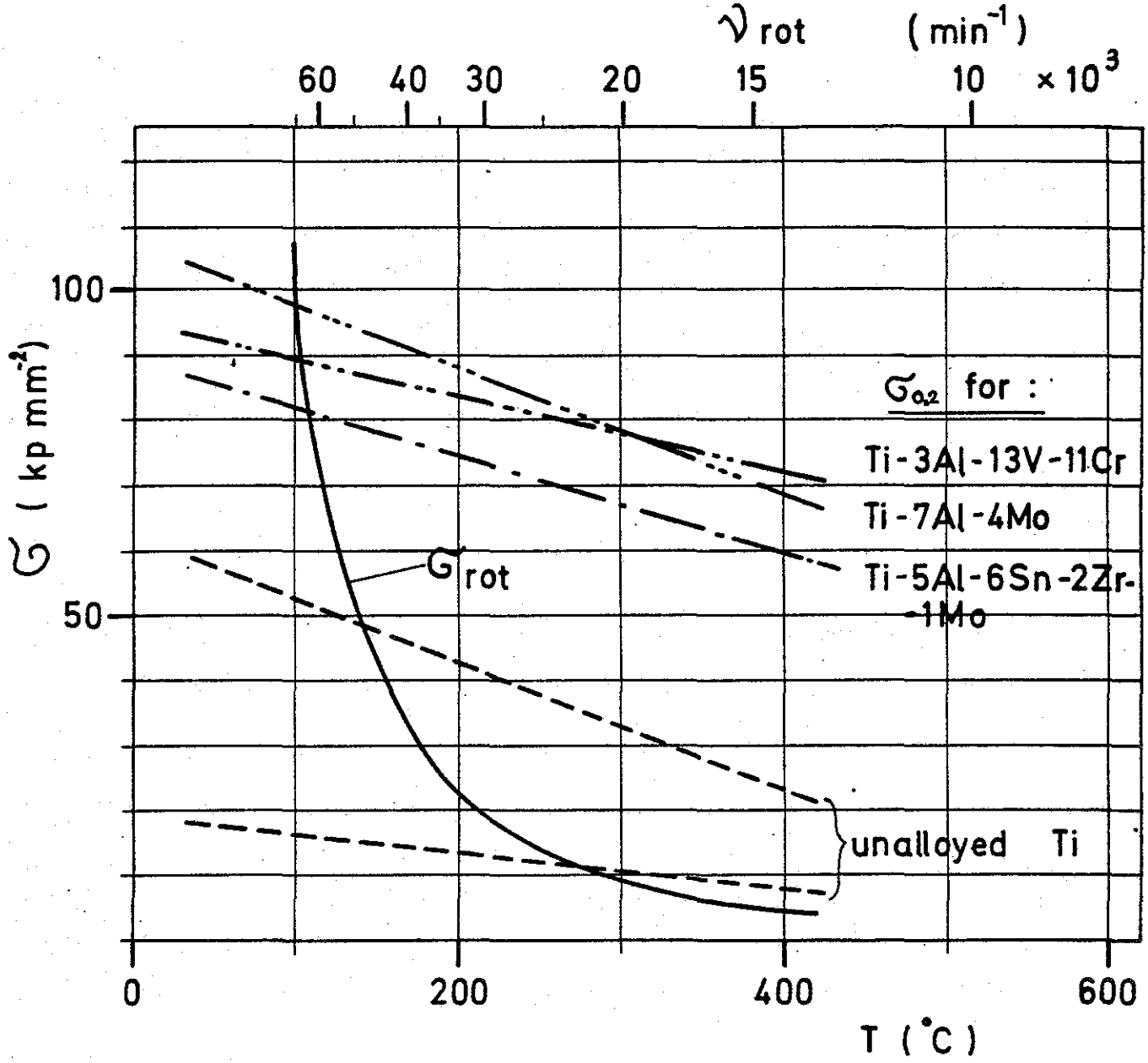

Fig. 9 The maximum stress σ_{rot} which occurs in a solid titanium cylinder due to its rotation is shown as a function of the temperature rise T at the beam axis. The upper abscissa gives the corresponding rotation frequences ν_{rot} for a cylinder of 20 cm diameter. For comparison also the yield strength $\sigma_{0.2}$ is shown for pure titanium (the values are ranges for five grades of unalloyed titanium with purity of 98.9 - 99.5 %) and three of its alloys. The numbers before the symbols indicate the percentage of the alloy constituents.

Monte Carlo programme [5]. Their precision is limited to the extent that this programme correctly describes the development of nucleon-meson cascades initiated in matter by primary protons up to 400 GeV/c. The expected precision of the energy deposition density calculated with the FLUKA programme is estimated to be 50% or better [8].

For targets cooled by either conduction or forced gas convection, e.g. with helium, it has been shown that acceptable target temperatures can be obtained for slow and fast extracted beams.

Furthermore, the problem of thermal stress has been examined.

Only in targets exposed to fast extracted or fast slow extracted beams with a spill duration shorter than 50 ms thermal stress becomes important. However, the dynamic stress can be reduced to values well below the yield strength of the heated material, if the target of a total length of typically one interaction mean-free path is subdivided into several parts. Moreover, it has been shown that the quasi-static thermal stress due to the radially non-uniform heating of a target causes the most serious problem, since the target material becomes plastic in the target core along the beam axis.

Among the ways to overcome this problem of the quasi-static thermal stress two suggested solutions are rather obvious :

- A blow-up of the beam waist by approximately a factor 4 would reduce the quasi-static thermal stress to values below the yield strength of the target material. However, this may be unacceptable in some cases for reasons of secondary beam optics.

- For targets of transverse dimensions approximately one order of magnitude larger than the beam diameter, the plastic region in the target centre is still surrounded by sufficient elastic material. Therefore, a reliable target operation may be expected, unless the lifetime is reduced to an unacceptably short duration due to the

repeated overstressing of the material along the target axis.

Furthermore, some unorthodox target constructions have been studied in case the above mentioned suggestions are unacceptable. However, there are still some problems to be investigated for each of these target constructions proposed for the operation in fast or fast slow extracted beams :

- For the granular target the problem is to find reliable container windows close to the target material. This is particularly difficult for the exit window, as it is traversed by the secondary particles as well as by the non-absorbed primary protons.

- In the case of the carbon fibre target the performance of the filaments repeatedly exposed to high temperatures must be investigated.

- For fast slow extracted beams with a spill time down to a few milliseconds a rotating cylindrical target with a rotation frequency of about 2000 revolutions per minute is technically possible. For fast extracted beams, however, the required rotation frequencies of about $2 \cdot 10^4$ revolutions per minute are far too high for a reliable target construction.

ACKNOWLEDGEMENTS

The authors wish to thank all colleagues who through discussions have contributed to this paper. In particular, we want to thank H. Bargmann J. Ranft, J.T. Routti and K. Teutenberg for enlightening discussions.

LITERATURE

1. H. Bargmann, Dynamic response of external targets under thermal shock, CERN-LAB II/BT/Int./73-3 (1973).

2. P. Sievers, Elastic stress waves in matter due to rapid heating by an intense high energy particle beam, CERN-LAB II/BT/74-2 (1974).

3. S.P. Timoshenko and J.N. Goodier, Theory of elasticity, 3rd edition, McGraw-Hill Book Company, New-York (1970).

4. The 300 GeV Programme, CERN/1050/72 (1972).

5. J. Ranft and J.T. Routti, FLUKA and MAGKA, Monte Carlo programs for calculating nucleon-meson cascades in cylindrical geometries, CERN-LAB II/RA/71-4 (1971).

6. G. Belletini, G. Cocconi, A.N. Diddens, E. Lillethun, G. Matthiae, J.P. Scanlon and A.M. Wetherell, Proton-nuclei cross-sections at 20 GeV, Nucl. Phys. 79 (1966) 609.

7. J.T. Routti and P. Sievers, Radiation heating of the vacuum chamber, CERH-LAB II/Note/72-19 (1972).

8. J. Ranft, private communication.

9. SPS Experimental Facilities, CERN/SPC/345(a) (1973).

10. VDI-Wärmeatlas, VDI-Verlag G.m.b.H., Düsseldorf, 1963.

11. M. Jacob, Heat transfer, Vol. I, J. Wiley & Sons, New-York, 1949.

12. W.H. Adams, Heat transmission, 3rd edition, McGraw-Hill Book Company, New-York, 1954.

13. K. Teutenberg, private communication.

14. Modmor Carbonfibres, Morganite Modmor Limited, London, England.

APPENDIX I

Gaussian beam profile

We assume that the radial distribution of the proton intensity over the beam cross-section may be represented by the following two-dimensional normalized Gaussian function:

$$W(r,\sigma) = \frac{1}{2\pi\sigma^2} \; e^{-(r^2/2\sigma^2)} \; ,$$

with

$$\int_0^{2\pi} \int_0^{\infty} W(r,\sigma) \; r \; dr \; d\phi = 1 \; ,$$

where r is the radial coordinate and σ the standard deviation of the radial beam profile. The probability that a proton is contained in an area of radius r is

$$w(r,\sigma) = 1 - e^{-(r^2/2\sigma^2)} \; .$$

A beam radius R_b is introduced to characterize the density distribution of a proton beam by a single parameter. R_b is defined such that 92% of the protons are contained in a cross-section of diameter $2R_b$. This leads to the following relation between R_b and σ:

$$R_b = 2.248 \; \sigma \; .$$

In this report the Monte Carlo calculations for the distribution of the energy deposition density are all made for a beam radius of R_b = 1 mm, which corresponds to a standard deviation σ = 0.445 mm.

APPENDIX II

Thermal stresses in cylindrical external targets

The following notations are used:

σ_r : radial stress component

σ_ϕ : circumferential stress component

σ_z : longitudinal stress component

σ^{dyn} : dynamic stress

σ^{stat} : quasi-static stress

$\sigma_{0.2}$: yield strength

E : Young's modulus

ν : Poisson's ratio

α : linear coefficient of thermal expansion

T(r) : radial temperature distribution suddenly superimposed on the initial uniform target temperature

r : radial coordinate

R : target radius

1. Dynamic thermal stress in the longitudinal direction of the target

Consider a stress-free, thin, elastic target cylinder which is freely suspended. Suppose, it is heated by one fast extracted pulse of 10^{13} ppp at 400 GeV/c. Then, owing to the extremely rapid temperature increase within 23 μsec, dynamic stress becomes important (see section 3.2.1). From Fig. 1 in Chapter 2 it follows that the temperature distribution in the target is approximately uniform over its length, but radially the temperature decreases rapidly. The quasi-static longitudinal stress produced by the radial temperature gradient is given by the following formula[3]:

$$\sigma_z^{stat} = \frac{\alpha E}{1-\nu}\left(\frac{2}{R^2}\int_0^R T(r)\, r\, dr - T(r)\right). \qquad (IV.1)$$

The longitudinal dynamic stress is obtained from the difference of the stresses in an axial free (σ_z^{stat}) and an axial constrained ($\sigma_z'^{stat}$) target cylinder with[3)]

$$\sigma_z'^{stat} = \nu\frac{\alpha E}{1-\nu}\left(\frac{2}{R^2}\int_0^R T(r)\, r\, dr - T(r)\right) - E\alpha\, T(r). \qquad (IV.2)$$

Thus, the maximum dynamic stress, i.e. the stress which occurs immediately after the fast heating of the target, in the longitudinal direction is:

$$\sigma_z^{dyn} = \pm(\sigma_z^{stat} - \sigma_z'^{stat}) = \pm E\alpha\,\frac{2}{R^2}\int_0^R T(r)\, r\, dr\,. \qquad (IV.3)$$

The dynamic stress σ_z^{dyn} is now calculated for three different temperature distributions T(r) which are each suddenly superimposed on the initial uniform target temperature.

Temperature distribution 1

Consider a target, suddenly heated, in which the temperature is increased uniformly through the target volume with T_0, i.e.

$$T(r) = T_0 = \text{constant}.$$

Then, the maximum value for the dynamic stress is[1,2)]:

$$\sigma_z^{dyn} = \pm E\alpha T_0\,.$$

Temperature distribution 2

Consider a temperature distribution which decreases linearly from the maximum temperature T_0 at the target centre to zero at the radial distance R', and is constant for $R' \leq r \leq R$:

$$T(r) = \begin{cases} T_0 \left(1 - \frac{r}{R'}\right) & 0 \leq r \leq R' \\ 0 & R' \leq r \leq R \, . \end{cases}$$

The corresponding dynamic stress is given by

$$\sigma_z^{dyn} = \pm \frac{1}{3} E\alpha T_0 \left(\frac{R'}{R}\right)^2 \, .$$

In the case of a Gaussian distribution of the proton intensity characterized by a beam radius of 1 mm, the range of the linear temperature distribution approximately coincides with this value. Thus, for slender targets of about 2 mm diameter, the dynamic stress is

$$\sigma_z^{dyn} \approx \frac{1}{3} E\alpha T_0 \, .$$

Temperature distribution 3

Consider a temperature distribution which consists of a linearly decreasing temperature in the inner interval $0 \leq r \leq R'$, and a variation proportional r^{-2} in the outer interval $R' \leq r \leq R$:

$$T(r) = \begin{cases} T_0 - (T_0 - T') \frac{r}{R'} & 0 \leq r \leq R' \\ T' \left(\frac{R'}{r}\right)^2 & R' \leq r \leq R \, . \end{cases}$$

Then, the integration of Eq. (IV.3) yields for the maximum dynamic stress:

$$\sigma_z^{dyn} = \pm \frac{E\alpha T_0}{3} \left(\frac{R'}{R}\right)^2 \left\{1 + 2 \frac{T'}{T_0} \left[1 + 3 \ln (R/R')\right]\right\}.$$

To compare this result with the one obtained for the temperature distribution 2, we assume, for instance, $R/R' = 2$ and $T_0/T' = 10$, which leads to

$$\sigma_z^{dyn} = \pm 0.4 \frac{E\alpha T_0}{3} \quad .$$

The last temperature distribution gives a good approximation of the target temperature obtained from the Monte Carlo programme (see Chapters 2 and 3) for a beam with a Gaussian density distribution, particularly for targets with a diameter larger than the beam diameter.

However, the maximum dynamic stress $\sigma_z^{dyn} = \pm \frac{1}{3} E \alpha T_0$, calculated for the temperature distribution 2, and $R' = R$ yields a reasonable upper limit of longitudinal dynamic stresses produced by a fast extracted proton pulse in slender target cylinders.

2. Quasi-static thermal stress in the longitudinal direction of the target

The longitudinal component of the quasi-static thermal stress produced in a cylindrical target, freely suspended, is calculated now with Eq. (IV.1) for each of the temperature distributions 1 to 3:

Temperature distribution 1 $\qquad \sigma_z^{stat} = 0$

Temperature distribution 2

The maximum of the quasi-static stress σ_z^{stat} is reached at the target centre:

$$\sigma_z^{stat} = - \frac{E\alpha T_0}{1 - \nu} \left[1 - \frac{1}{3} \left(\frac{R'}{R}\right)^2\right] \quad \text{for } r = 0 \ .$$

For $R = R'$ respectively $R \gg R'$ the limiting values of this quasi-static stress are

$$\sigma_z^{stat} = \begin{cases} -\frac{2}{3}\frac{E\alpha T_0}{1-\nu} \approx -E\alpha T_0 & \text{for } R = R' \\ -\frac{E\alpha T_0}{1-\nu} \approx -\frac{3}{2} E\alpha T_0 & \text{for } R \gg R' . \end{cases}$$

Temperature distribution 3

$$\sigma_z^{stat} = -\frac{E\alpha T_0}{1-\nu}\left[1 - \frac{1}{3}\left(\frac{R'}{R}\right)^2 \left\{1 + 2\frac{T'}{T_0}\left[1 + 3\ \ln\ (R/R')\right]\right\}\right] \quad \text{for } r = 0 .$$

The maximum of the quasi-static stress for $R = R'$ respectively $R \gg R'$ then is

$$\sigma_z^{stat} = \begin{cases} -\frac{2}{3}\frac{E\alpha T_0}{1-\nu}\left(1 - \frac{T'}{T_0}\right) \approx -E\alpha T_0\left(1 - \frac{T'}{T_0}\right) & \text{for } R = R' \\ -\frac{E\alpha T_0}{1-\nu} \approx -\frac{3}{2} E\alpha T_0 & \text{for } R \gg R' . \end{cases}$$

3. Calculation of the radius of the central plastic core

The central plastic core produced by quasi-static thermal stress is defined by the radius for which the absolute value of the maximum difference between the stress-components is equal to the yield strength of the target material considered:

$$\sigma_{0.2} = \sigma_0 \equiv \max \begin{cases} |\sigma_\phi - \sigma_r| \\ |\sigma_\phi - \sigma_z| \\ |\sigma_r - \sigma_z| \end{cases} .$$

The stress components in cylindrical targets, freely suspended, can be evaluated with the following formulae:

$$\sigma_r^{stat} = \frac{\alpha E}{1-\nu}\left[\frac{1}{R^2}\int_0^R T(r)\, r\, dr - \frac{1}{r^2}\int_0^r T(r)\, r\, dr\right]$$

$$\sigma_\phi^{stat} = \frac{\alpha E}{1-\nu}\left[\frac{1}{R^2}\int_0^R T(r)\, r\, dr + \frac{1}{r^2}\int_0^r T(r)\, r\, dr - T(r)\right];$$

σ_z^{stat} was already given above [Eq. (IV.1)].

For each of the temperature distributions 1 to 3 we have derived the formulae for the calculation of the radius δ of the central plastic core:

Temperature distribution 1

$$\delta_1 \equiv 0 .$$

Temperature distribution 2

$$\delta_2 = R' \sqrt{\frac{1}{3}\,\frac{E\alpha T_0}{(1-\nu)\,\sigma_{0.2}}} .$$

Temperature distribution 3

$$\delta_3 \approx \delta_2 \left\{1 + \frac{T'}{T_0}\left[6 \ln (\delta_2/R') - 1\right]\right\}^{1/2} .$$

APPENDIX III

Convection coefficients for horizontal cylinders[10,11,12]

In this appendix the following variables are used:

k_{conv}	:	convection coefficient	(cal cm^{-2} sec^{-1} $°C^{-1}$)
d	:	outer diameter of the cylinder	(m)
λ	:	thermal conductivity	(kcal m^{-1} h^{-1} $°C^{-1}$)
c	:	specific heat	(kcal kg^{-1} $°C^{-1}$)
g	:	gravitational constant = 9.81	(m sec^{-2})
η	:	dynamic viscosity	(kg sec m^{-2})
γ	:	specific weight	(kg m^{-3})
β	:	coefficient of thermal expansion	($°C^{-1}$)
Δt	:	temperature difference between cylinder surface t_w and mean gas temperature t_m	(°C)
v	:	velocity of the gas	(m sec^{-1})

This notation is restricted to this part of the appendix as, in general, it is different from the one used in the other parts of this report!

The calculation for the convection coefficient is facilitated by a set of dimensionless numbers:

Nusselt $Nu = 3.6 \times 10^4 \frac{k_{conv} \cdot d}{\lambda}$

Prandtl $Pr = 3.6 \times 10^3 \frac{c \cdot g \cdot \eta}{\lambda}$

Grashof $Gr = \frac{\gamma^2 \beta \Delta t \cdot d^3}{\eta^2 \cdot g}$

Reynolds $Re = \frac{v \cdot \gamma \cdot d}{\eta \cdot g}$.

The most general correlation between these dimensionless numbers is given by

$$Nu = C \cdot Re^m \cdot Pr^n \cdot Gr^r .$$

The exponents m, n, and r and the constant C can be determined theoretically and/or experimentally depending on the complexity of the special problem.

Natural convection coefficients

Measurements of Jodlbauer and theoretical calculations of Hermann resulted in[10)]

$$Nu = 0.40 \cdot \sqrt[4]{Gr \cdot Pr} \quad . \qquad (II.1)$$

This equation should be applied in the following interval:

$$10^5 \leq Pr \cdot Gr < 10^8 \, .$$

For $Pr \cdot Gr < 10^5$, which is mostly the case of thin cylinders such as external targets, a diagram (Fig. 10) given by Senftleben[10)] should be used.

The values for the gas constants are to be taken at the temperature t_w of the cylinder surface; only the parameter β has to be evaluated at the mean temperature t_m of the gas.

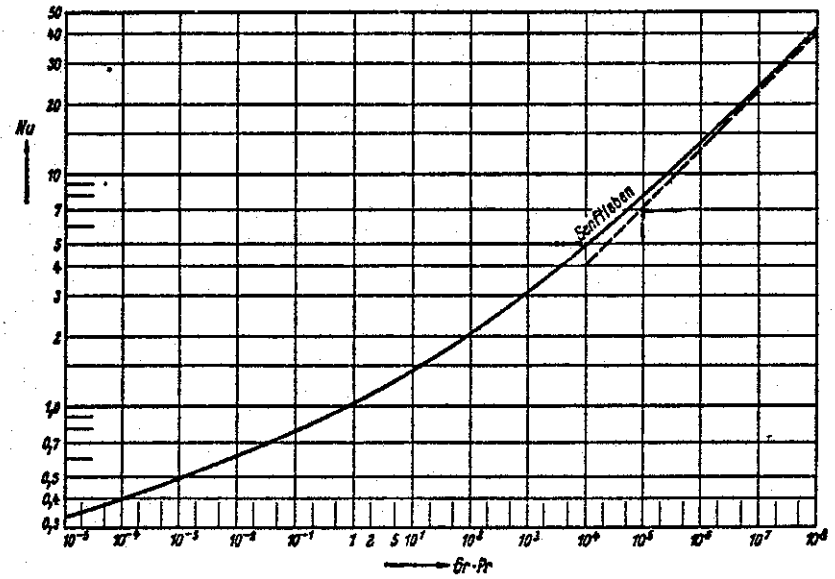

Fig. 10 Heat transfer by natural convection for horizontal cylinders. The solid curve is given by Senftleben and the dashed line is calculated from Eq. (II.1).

Forced convection coefficients

For a transversal gas stream, Ulsamer and Hilpert have given the following formula[10]:

$$Nu = 1.11 \cdot C \cdot Re^{m} \cdot Pr^{0.31} \cdot (0.785 \cdot T_w/T_m)^{m/4} . \qquad (II.2)$$

This equation is valid in the following intervals:

$$0.1 \leq Re \leq 10^6$$

$$0.5 \leq Pr \leq 10^3 .$$

The values for the material constants are to be taken at the temperature

$$\frac{1}{2}\left(t_w + \frac{t' + t''}{2}\right)$$

t_w : temperature of the cylinder (°C)

T_w : temperature of the cylinder (°K)

t' : temperature of the incoming gas (°C)

t'' : temperature of the outgoing gas (°C)

T_m : temperature of the incoming gas (°K) .

The parameters C and m as a function of the Reynolds number are listed in the table:

from Re	to	C	m
0.4	4	0.891	0.330
4	40	0.821	0.385
40	4000	0.615	0.466
4000	40000	0.174	0.618
40000	400000	0.0239	0.805

Table XIII Constants of Eq. (II.2) for forced convection perpendicular to cylinders.

APPENDIX IV

Steady-state temperatures in external targets for cooling by convection only

The following notation is used in this appendix:

t : time counted from the beginning of a machine cycle

τ : burst length

τ_R : repetition period

T : uniform temperature of the target

T_m : temperature of the cooling medium (gas)

Θ : target temperature relative to the temperature of the cooling medium ($T-T_m$)

$\Theta_{n\tau}$: target temperature at the end of the n^{th} burst

Θ_{nR} : target temperature at the end of the n^{th} thermal cycle

V : target volume

S : target surface

R : target radius

ρ : mass density

c_p : specific heat

Q_0 : total heat produced in a target by 10^{13} ppp of 400 GeV/c

k_{conv} : convection coefficient

The variation of the target temperature is considered here only for times which are long compared with the thermal diffusion time. Therefore, uniform target temperatures can be assumed. For an external target, that is heated by a pulsed proton beam and cooled by convection only, the following differential equations describe the time-dependent variation of the uniform target temperature T :

i) during the burst, when the target is simultaneously heated and cooled:

$$\frac{Q_0}{\tau} = c_p \cdot \rho \cdot V \cdot \frac{dT}{dt} + k_{conv} \cdot S \cdot (T - T_m) \qquad 0 \leq t \leq \tau \; ; \; (III.1)$$

ii) between two bursts when the target is only cooled:

$$0 = c_p \cdot \rho \cdot V \cdot \frac{dT}{dt} + k_{conv} \cdot S \cdot (T - T_m) \qquad \tau \leq t \leq \tau_R \; . \qquad (III.2)$$

This is a special case of the equations (4a) and (4b) given in Section 4.2.1.

Introducing $\Theta \equiv T - T_m$ into Eqs. (III.1) and (III.2), the temperature variation during the first thermal cycle becomes, after integration,

$$\Theta = T_\infty \, (1 - e^{-\xi t}) \qquad 0 \leq t \leq \tau$$

$$\Theta = T_\infty \, (1 - e^{-\xi \tau}) \, e^{-\xi (t-\tau)} \qquad \tau \leq t \leq \tau_R \; ,$$

where

$$\xi = \frac{k_{conv} \, S}{c_p \, \rho \, V} = \frac{2 \, k_{conv}}{c_p \, \rho \, R}$$

$$T_\infty = \frac{Q_0}{\tau \, S \, k_{conv}} \; .$$

Then the target temperatures at the end of the first burst and the first thermal cycle, respectively, are given by

$$\Theta_{1\tau} = T_\infty \, (1 - e^{-\xi \tau}) \qquad , \quad t = \tau$$

$$\Theta_{1R} = T_\infty \, (1 - e^{-\xi \tau}) \, e^{-\xi (\tau_R - \tau)} , \quad t = \tau_R \; .$$

Now the following recursion formulae for the n^{th} pulse can be derived:

$$\Theta_{n\tau} = \Theta_{1\tau} \sum_{m=0}^{n-1} e^{-m\xi\tau_R}, \quad t = n\,\tau_R + \tau$$

$$\Theta_{nR} = \Theta_{1R} \sum_{m=0}^{n-1} e^{-m\xi\tau_R}, \quad t = (n+1)\tau_R \,.$$

As $\xi \cdot \tau_R > 0$, the following limit is obtained:

$$\lim_{n\to\infty} \sum_{m=0}^{n-1} e^{-m\xi\tau_R} = \frac{1}{1 - e^{-\xi\tau_R}} \,.$$

Therefore, the steady-state temperatures at the end of a burst Θ_τ and a thermal cycle Θ_R are given, respectively, by

$$\Theta_\tau = T_\infty \frac{1 - e^{-\xi\tau}}{1 - e^{-\xi\tau_R}}$$

$$\Theta_R = T_\infty \frac{1 - e^{\xi\tau}}{1 - e^{\xi\tau_R}} \,.$$

The ratio of both temperatures is

$$\frac{\Theta_\tau}{\Theta_R} = e^{\xi(\tau_R - \tau)} \,.$$

In the case of fast extraction or of slow extraction with an extremely short spill time of about 1 msec the cooling of the target may well be neglected during the burst length as $\tau \ll \tau_R$. Therefore in the limit of $\tau \to 0$ a simpler formula can be derived:

$$\tilde{\Theta}_R = \lim_{\tau \to 0} \Theta_R = \frac{Q_0}{k_{conv} \cdot S \cdot (1 - e^{\xi \tau_R})} \lim_{\tau \to 0} \frac{1 - e^{\xi \tau}}{\tau}$$

$$= \frac{\xi \cdot Q_0}{k_{conv} \cdot S \cdot (1 - e^{\xi \tau_R})}$$

$$\tilde{\Theta}_R = \frac{\bar{T}}{e^{\xi \tau_R} - 1} \quad ,$$

where $\bar{T} = Q_0 / c_p \cdot \rho \cdot V$ is the fast rise of the uniform target temperature due to one proton pulse.

The formulae, derived above for the steady-state temperatures, calculate the difference between the target temperatures and the temperature of the cooling medium T_m. Therefore the absolute values of the target temperatures become:

$$T_\tau = T_\infty \frac{1 - e^{-\xi \tau}}{1 - e^{-\xi \tau_R}} + T_m$$

$$T_R = T_\infty \frac{1 - e^{\xi \tau}}{1 - e^{\xi \tau_R}} + T_m$$

$$\tilde{T}_R = \frac{\bar{T}}{e^{\xi \tau_R} - 1} + T_m \quad .$$